NUMERICAL SIMULATION OF QUARRY BLAST SOURCES

T. G. Barker
K. L. McLaughlin
J. L. Stevens

Maxwell Laboratories, Inc.
S-CUBED Division
P.O. Box 1620
La Jolla, CA 92038-1620

January 1993

Technical Report

Phillips Laboratory
Kirtland Air Force Base, NM 87117-5320

The views and conclusions contained in this report are those of the authors and should not be interpreted as representing the official policies, either expressed or implied, of the Defense Advanced Research Projects Agency or the U.S. Government.

REPORT DOCUMENTATION PAGE

Form Approved
OMB No. 0704-0188

1. AGENCY USE ONLY *(Leave blank)*	2. REPORT DATE	3. REPORT TYPE AND DATES COVERED
	1 January 1993	Technical Report 9/18/91-11/1/92

4. TITLE AND SUBTITLE

NUMERICAL SIMULATION OF QUARRY BLAST SOURCES

5. FUNDING NUMBERS

F29601-91-C-DB27

6. AUTHOR(S)

T. G. Barker, K. L. McLaughlin and J. L. Stevens

7. PERFORMING ORGANIZATION NAME(S) AND ADDRESS(ES)

Maxwell S-CUBED Division
P.O. Box 1620
La Jolla, CA 92038-1620

8. PERFORMING ORGANIZATION REPORT NUMBER

SSS-TR-93-13859

9. SPONSORING/MONITORING AGENCY NAME(S) AND ADDRESS(ES)

DARPA-NMRO
3701 N. Fairfax Dr. #717
Arlington, VA 2203-1714

Phillips Laboratory (PL/PKVA)
3651 Lowry Avenue, SE
Kirtland, AFB, NM 87117-5777

10. SPONSORING/MONITORING AGENCY REPORT NUMBER

11. SUPPLEMENTARY NOTES

12a. DISTRIBUTION/AVAILABILITY STATEMENT

Approved for Public Release; Distribution Unlimited

12b. DISTRIBUTION CODE

13. ABSTRACT *(Maximum 200 words)*

Quarry blast sources are developed based on well-documented blasting practices from decades of blasting in quarries and used to simulate seismic signals from quarry blasts, and to examine the "hide-in-quarry blast" scenario for evading detection of nuclear weapons testing. Blasting is designed to break rock through spallation, and the resultant spall is an important part of the quarry blast source. The quarry blast source models include the finite size of the source, the effect of ripple firing (time delays and spatial separation), the effect of net vertical and horizontal rock movement, and the relative excitation of the explosion and spall sources. We simulate the "hide-in-quarry blast" scenario as an overburied nuclear explosion beneath the quarry blast. We find that for a one kiloton quarry blast source:

1. The quarry blast source is band-limited compared to the buried explosion, and decays rapidly over the 0.5-3 Hz frequency band.

14. SUBJECT TERMS

Nuclear Discrimination
Synthetic Seismograms
Quarry Blast
Nuclear Testing

15. NUMBER OF PAGES

16. PRICE CODE

17. SECURITY CLASSIFICATION OF REPORT	18. SECURITY CLASSIFICATION OF THIS PAGE	19. SECURITY CLASSIFICATION OF ABSTRACT	20. LIMITATION OF ABSTRACT
UNCLASSIFIED	UNCLASSIFIED	UNCLASSIFIED	

CLASSIFIED BY:

DECLASSIFY ON:

13. Abstract *(Continued)*

2. Pg spectral values rise in the band from 0.5 to 3.5 Hz for the bomb, but fall in that band for the quarry blast.
3. Spall strongly affects the quarry blast source enhancing the generation of Pg and Lg.
4. In a simultaneous explosion and quarry blast, the explosion will dominate the seismic signal if the explosion yield (tamped or equivalent decoupled) exceeds approximately 10 percent of the quarry blast yield.
5. Quarry blast spectral scallops are primarily due to the finite size and duration of the source and are insensitive to the details of the ripple firing timing.
6. Seismic amplitudes from quarry blasts are insensitive to the direction of spall as long as there is minimal elevation change.
7. An elevation change (the spalled quarry face falling to a lower level) can significantly increase seismic amplitudes from quarry blasts. An elevation drop of 10 meters can increase the quarry blast signal by as much as a factor of 5 in the 2-5 Hz freqency band.

Table of Contents

Section **Page**

List of Illustrations

List of Illustrations (Cont.)

List of Illustrations (Cont.)

Summary

Quarry blast sources are developed based on well-documented blasting practices from decades of blasting in quarries and used to simulate seismic signals from quarry blasts, and to examine the "hide-in-quarry blast" scenario for evading detection of nuclear weapons testing. Blasting is designed to break rock through spallation, and the resultant spall is an important part of the quarry blast source. The quarry blast source models include the finite size of the source, the effect of ripple firing (time delays and spatial separation), the effect of net vertical and horizontal rock movement, and the relative excitation of the explosion and spall sources. We simulate the "hide-in-quarry blast" scenario as an overburied nuclear explosion beneath the quarry blast.

We find that for a one kiloton quarry blast source:

1. The quarry blast source is band-limited compared to the buried explosion, and decays rapidly over the 0.5-3 Hz frequency band.

2. Pg spectral values rise in the band from 0.5 to 3.5 Hz for the bomb, but fall in that band for the quarry blast,

3. Spall strongly affects the quarry blast source enhancing the generation of Lg and Pg.

4. In a simultaneous explosion and quarry blast, the explosion will dominate the seismic signal if the explosion yield (tamped or equivalent decoupled) exceeds approximately 10 percent of the quarry blast yield.

5. Quarry blast spectral scallops are primarily due to the finite size and duration of the source and are insensitive to the details of the ripple firing timing.

6. Seismic amplitudes from quarry blasts are insensitive to the direction of spall as long as there is minimal elevation change.

7. An elevation change (the spalled quarry face falling to a lower level) can significantly increase seismic amplitudes from quarry blasts. An elevation drop of 10 meters can increase the quarry blast signal by as much as a factor of 5 in the 2-5 Hz frequency band.

1. Introduction

It has been suggested that evading detection of nuclear weapons testing may be accomplished by detonating the weapons in conjunction with large quarry blasts. The objective of this project is to compare the regional seismic radiation from quarry blast sources and small, shallow, overburied nuclear explosions to determine whether it may be possible to discriminate between the two sources. Our approach is to use simple seismic models, derived from realistic numerical simulations and from field tests, as sources in synthetic seismogram calculations. We then examine synthetic seismograms and sonograms for discrimination features. In this report, we concentrate on the differences in regional seismic signals due to differences in source excitation, duration and size of the quarry blast and nuclear bomb sources. We find that these differences are reflected in observable features of the synthetic seismograms, and should be observable in field data.

We model the quarry blast as a series of shots distributed on a grid using a variety of temporal and spatial shot patterns. Each shot is a charge which creates a spalling of the material above, which is modeled as an explosion plus a set of forces associated with movement of the spall mass. In the following, we describe the quarry blast model in detail, and then focus on synthetic regional and teleseismic seismograms computed using the model.

2. Quarry Blast Models

2.1 Introduction

Blasting rock in quarries is done to fracture large rock masses and move the rock to where it can be loaded and hauled. Since quarrying by explosives is an old and widely practiced activity and has inherent safety concerns, standard practices used by mine operators have been developed which facilitate the removal of rock, mitigate vibrations to surrounding structures and improve safety. In this section, we review standard practices that are pertinent to the generation of seismic waves and then describe how we have incorporated these practices into our models.

2.2 Blasting Practices

For this report, we consider the scenario that an evader wishes to hide a nuclear explosion under a large simultaneous chemical quarry blast. In our simulations we have used a quarry blast with a total yield of 1 kiloton and nuclear explosions with equivalent yields of 0.1 and 1 kiloton.

The spatial scale of the quarry blast can be estimated from the total explosive yield and from standard blasting practices. Most quarrying is done by removing material from the face of a bench using multiple rows of charges parallel to the bench. This geometry is shown schematically in Figure 1. The largest bench height in practice is about 30 m (Langefors and Kihlstrom, 1963). The burden Q (distance from the face of the bench to the charge) is, as a rule, one-half the bench height, (Langefors and Kihlstrom, 1963, Dupont, 1942), or about 15 m. The standard spacing between holes in a row as well as the spacing between rows is about 1.25 times the burden. The standard charge size (per hole) is 0.6 Q^3 Kg, or 2025 Kg, or about two metric tons for a 15 m burden. So, if the total charge is one kiloton, the total number of holes is 500. In the calculations described here, we used 20 rows with 25 charges per row, covering an area of roughly 300 m by 450 m, as shown in Figure 2.

The charges are detonated in firing patterns that vary with the requirements and constraints of the quarry. The most typical pattern is to fire the shots within a row simultaneously or at very short intervals, and detonate the

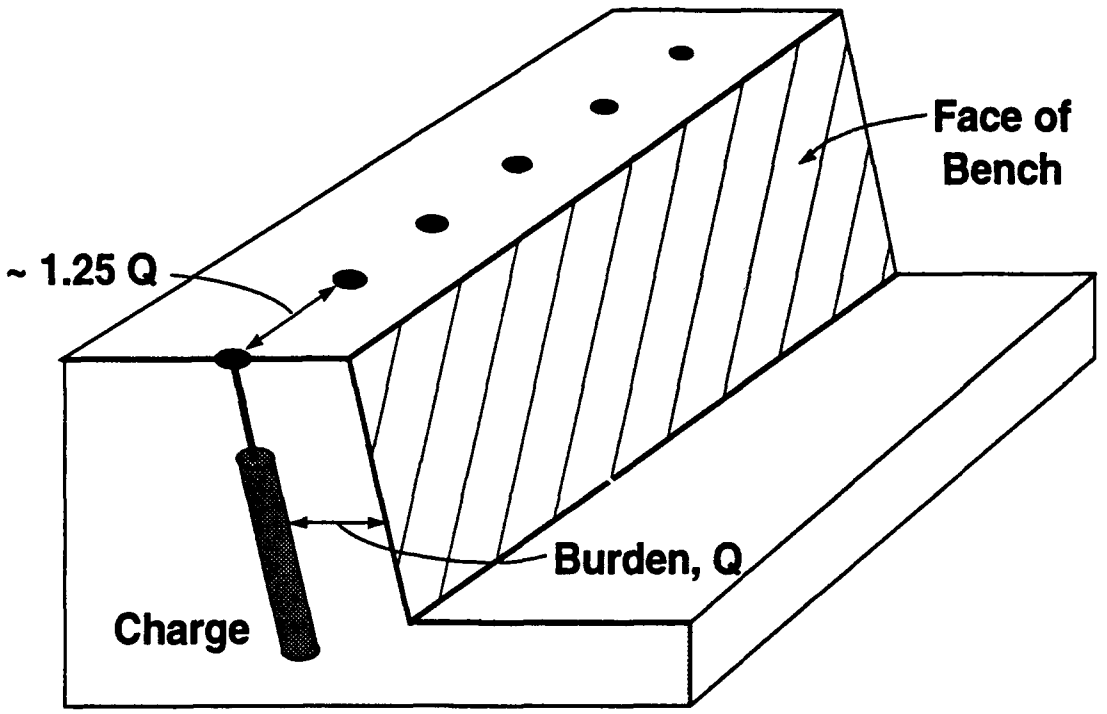

Figure 1. Schematic drawing of a row of charges at the face of a quarry blast.

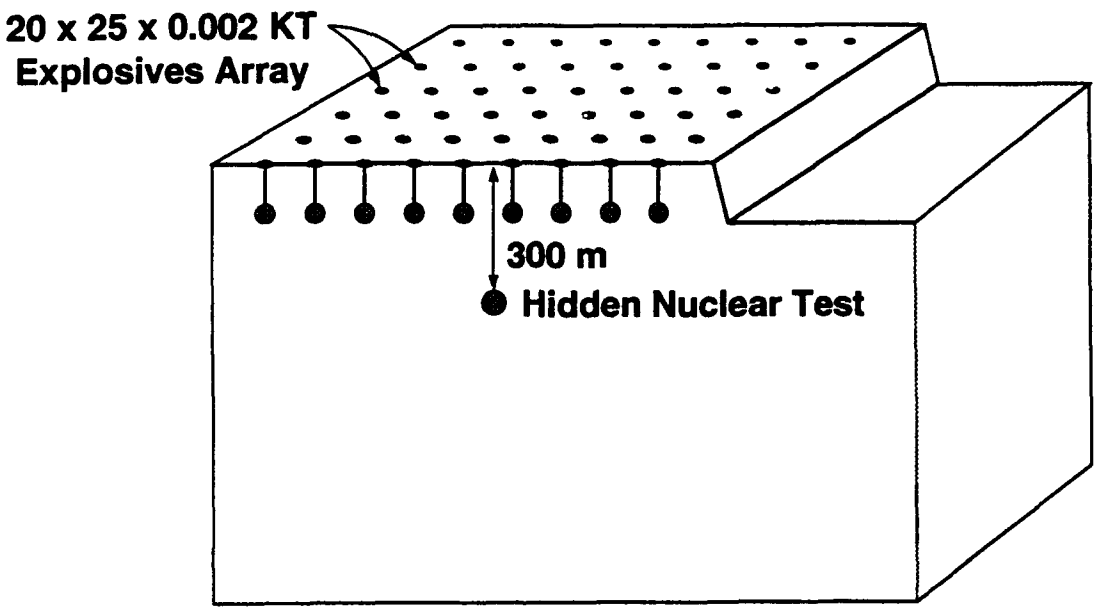

Figure 2. Schematic drawing of the quarry blast model. Calculations were performed for a 1 kiloton quarry blast over a clandestine nuclear test with yields of 0.1 and 1 kilotons. A 0.1 kiloton tamped explosion generates signals comparable to a fully decoupled 7 kiloton explosion or a smaller partially coupled explosion (see Section 2.4).

rows at even intervals beginning with the row nearest the face. The intervals between rows are a few tenths of a second. The objective of progressive firing within a row is to encourage gas driven fracture between holes to make the rock separate more readily along a line between the holes. The rows are fired at intervals so that the rocks thrown from a particular row do not interfere with the detachment of the subsequent row.

Chapman, *et al.* (1991) examined the drilling practices of quarries in eastern Kentucky. The charge pattern for an excavation with a total yield of 0.115 KT is shown in Figure 3. In this case, there were 56 charges arranged in 4 rows of 14. The charge size per hole was 1.87 metric tons. The spacing is about 12 m between shots within a row and about 8 m between rows (0.65 Q^3 Kg). This pattern is similar to other charge patterns shown in their report. Since there is a practical upper limit of about two metric tons per hole (determined by the maximum practical bench height, as discussed above), a larger yield can be achieved only by increasing the number of holes. If the example in Figure 3 were to be scaled up to 1 KT, the number of holes would be increased to around 500. The detonation times are also indicated in Figure 2. Each row was initiated at the center and the duration of firing in each row is 165 msec. The interval between rows was about 250 msec, the total duration of the blast was 0.78 sec, and the area covered by charges was 150m x 35m.

Experience in blasting has shown that charge sizes of 1 to 2 Kg/Q^3 (burden Q in meters) are optimal for safety and for providing the needed displacement of the burden. This corresponds to scaled burdens of between 0.5 and 1 $m/Kg^{1/3}$, or 50 to 100 $m/KT^{1/3}$. Nuclear explosions are generally buried at scaled depths greater than 100 $m/KT^{1/3}$, historically with many explosions at "normal" depth of burial of 120 $m/KT^{1/3}$.

2.3 Model of the Quarry Blast Source

Material is removed from the face of a bench by a spall process in which the compressional wave from the explosives reflects from the face as a tension wave which causes the material to detach and become airborne. The spall process initiated by nuclear explosions has been modeled well by a tension crack (Day, *et al.*, 1983, Barker and Day, 1990, McLaughlin, *et al.*, 1990), and was used in Barker,

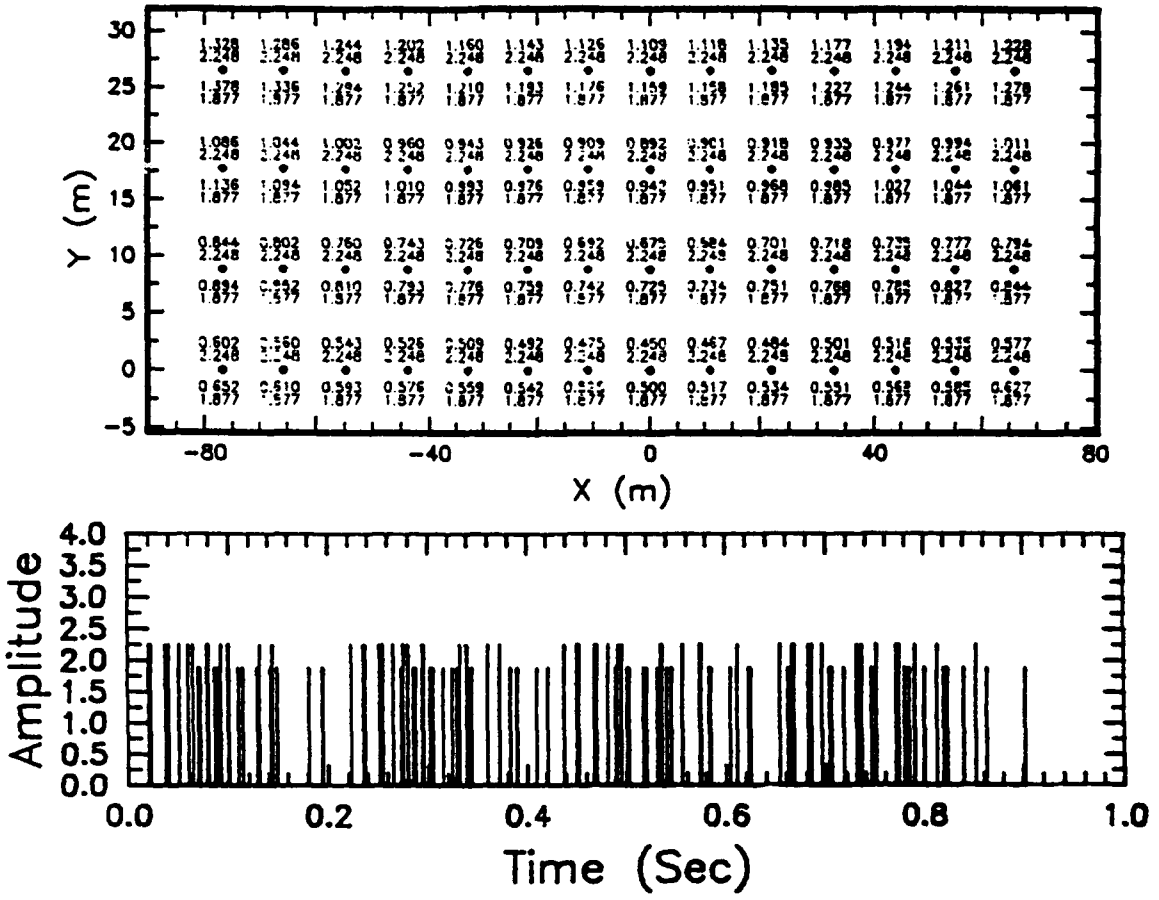

Figure 3. Example of a 0.1 KT quarry blast shot layout from Chapman, *et al.* (1991). (Top) Shot locations; written above each shot location are the charge size (in thousands of lbs) over the delay time in msec. (Bottom) shot size versus time.

et al. (1992) to model the quarry blast spall. In that work, the material was envisioned to lift vertically from a given depth and return to that depth. In the present paper, we provide for both lateral movement of the spalled material as well as net vertical movement, as shown in Figure 4. At each shot hole, there is an initial charge modeled as a Mueller-Murphy explosion source (Mueller and Murphy, 1971) plus point forces which represent the takeoff and landing of the spall mass. Stump and Reinke (1988) showed that the Mueller-Murphy source represents the explosive part of the signals from quarry blasts well. We assume that the depth where spall occurs is at the depth of the charge since firing patterns are designed to crack along a line through the charges (Langefors and Kihlstrom, 1963).

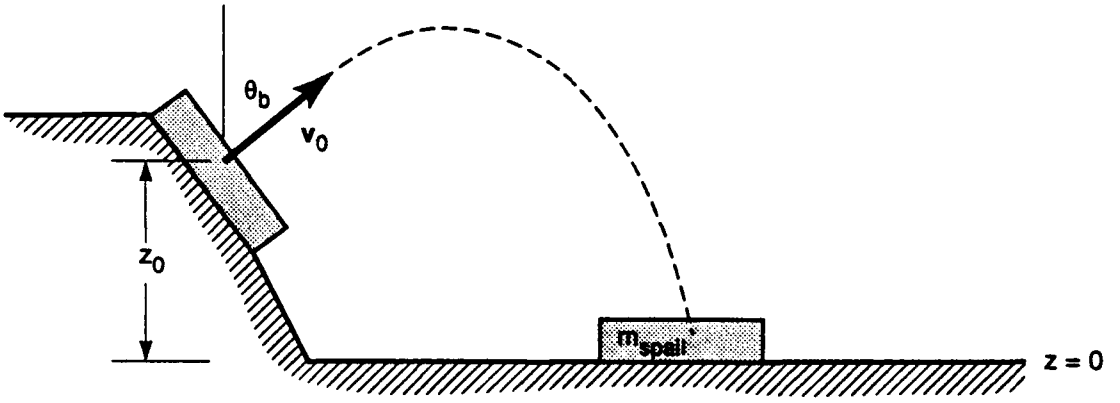

Figure 4. Schematic drawing showing movement of the spall mass.

The displacement due to movement of the spall mass is computed using

$$u_i(\underline{x},t) = F_j(\underline{x}_o,t) * g_i^j(\underline{x}-\underline{x}_o,t), \tag{1}$$

where F_j is the force exerted by the spall mass at $\underline{x}_o$, g_i^j is the displacement Green's function in the i^{th} direction due to a force in the j direction, and * denotes convolution. The force is simply

$$F_j(\underline{x}_o,t) = m_{spall}\frac{\partial^2}{\partial t^2} s_j(\underline{x}_o,t). \tag{2}$$

Here m_{spall} is the spall mass, and s_j describes the trajectory of the mass. For a mass given an initial upward velocity v_0 at an angle θ_b from the vertical at an initial height z_0 and falling to a height of z=0,

$$F_z(\underline{x}_o,t) = m_{spall}\left[\dot{z}_o\delta(t)+(g\,t_d-\dot{z}_o)\delta(t-t_d)-g\left(H(t)-H(t-t_d)\right)\right], \qquad (3)$$
$$F_x(x_o,t) = m_{spall}\,\dot{x}_o\left[\delta(t)-\delta(t-t_d)\right],$$

where

$$(\dot{x}_o,\dot{z}_o) = v_o(\sin\theta_b,\cos\theta_b)$$

and t_d is the dwell time, given by

$$t_d = g^{-1}\left[\dot{z}_o+\left(\dot{x}_o^2+2z_og\right)^{1/2}\right].$$

Equations (3) are shown graphically in Figure 5. The time $2\dot{z}_o/g$, marked on that figure, is the time required for the material to reach its peak and fall back to its initial height. The remaining part of the dwell time is spent falling to z=0. The effect of the initial height is to increase the amplitude of the second, or impact, delta function and increasing the duration of "unloading" force. The radial force is a force couple. Note that both the vertical and horizontal net forces are zero, showing that the model conserves momentum.

Barker, *et al.* (1992), computed the response from

$$u_i(\underline{x},t) = A_{spall}\ s_j(\underline{x}_o,t) * g_i^{TC}(\underline{x}-\underline{x}_o,t), \qquad (4)$$

where g_i^{TC} is the displacement Green's function due to a tension crack with area A_{spall}. Day and McLaughlin (1991), and McLaughlin, *et al.* (1992) (included as Appendix A) show that for wavelengths long compared to the tension crack depth z_{spall}

$$g_i^{TC}(\underline{x},t) = \rho\, z_{spall}\ \frac{\partial^2}{\partial t^2}\, g_i^z(\underline{x},t). \qquad (5)$$

Since $m_{spall} = \rho\, z_{spall}\, A_{spall}$, and since regional and teleseismic wavelengths are much longer than quarry burdens. Equation (4) is a good approximation of

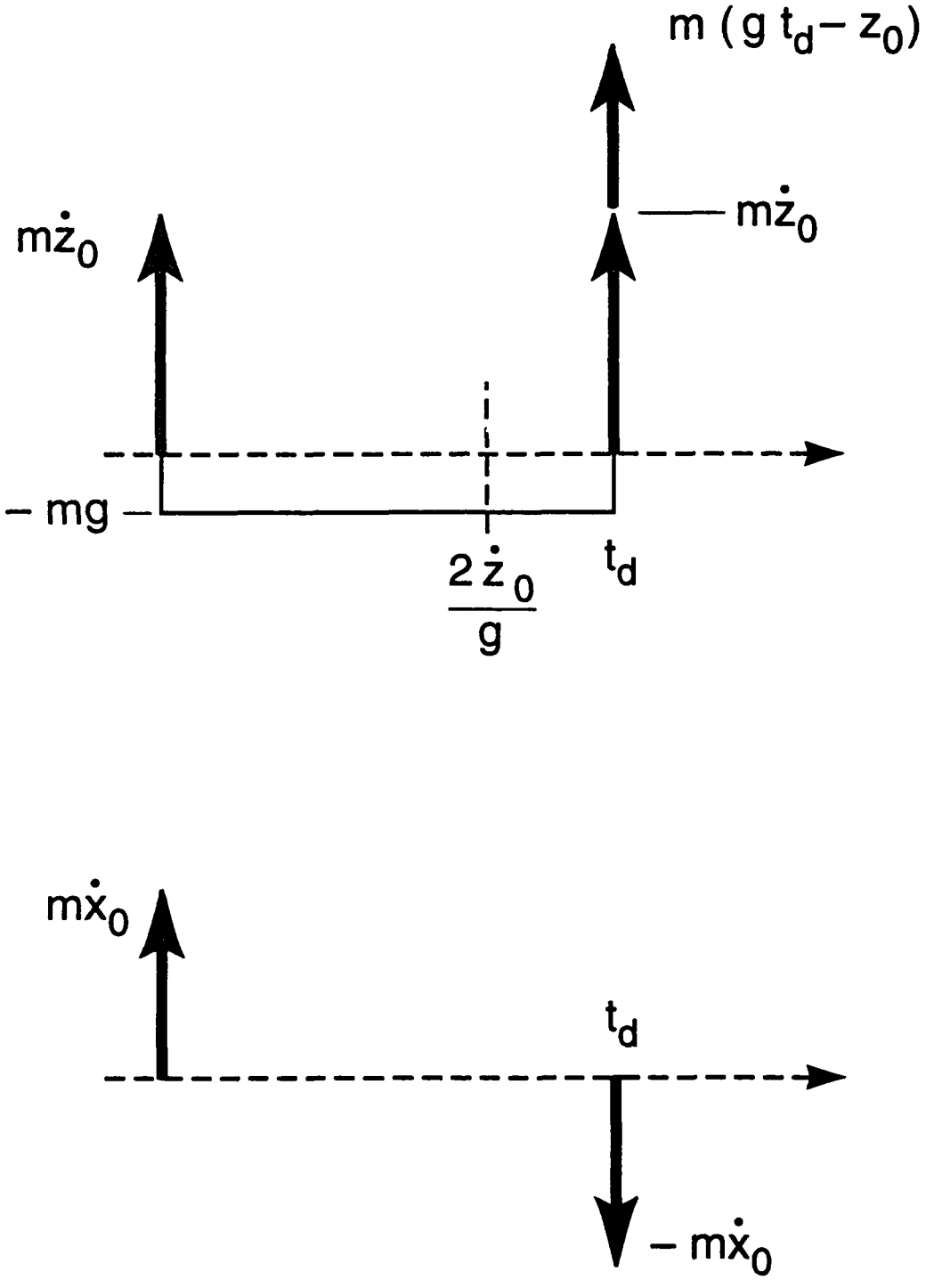

Figure 5. Graphic depiction of the vertical (top) and horizontal (bottom) spall force source functions (Equations 3).

Equation (1) when only vertical motion of the spall mass was considered, as was the case in Barker, *et al.* (1992).

2.3.1 Explosive Charge Model

The Mueller-Murphy source function describes the seismic radiation from a pressure source applied to the interior of a sphere. The source spectrum is flat at low frequencies and decays as f^{-2} above a corner frequency which is determined by the radius of the sphere (which in turn depends on other parameters of the model, such as yield and depth). Because the individual charges in a quarry blast are small (one ton), the corner frequency is above the regional seismic bandwidth, and the contributions of the charges to regional signals are affected only by the long period level. Since the scaling laws in the Mueller-Murphy source were derived for nuclear explosions, it is important to verify its validity for shallow, chemical explosions. McEvilly and Johnson (1989) (referred to here as M&J) have inferred the source strength of explosions in the Kaiser Permanente Quarry near Menlo Park, California, and Reamer, Hinzen and Stump (1992) (referred to as RH&S) have examined in detail an explosion in a limestone quarry in northern Italy. In Table 1, we summarize a comparison of source strengths (scaled moments and RDP, or Ψ_∞) in their studies and from Mueller-Murphy models at the same depths and yields. The moment and Ψ_∞ are not reported directly in RH&S, so we computed them from the reported values of elastic and cavity radii (which were inferred from their experiments using the Mueller-Murphy model) using the relations

$$P_0 = \frac{4}{3}\mu\left(\frac{r_c}{r_{el}}\right)^3 \tag{1}$$

$$\Psi_\infty = \frac{r_{el}c^2P_0}{4\mu\omega_0^2} \tag{2}$$

and

$$\omega_0 = \frac{c}{r_{el}} \tag{3}$$

Table 1
Source Strength Comparisons

Source	Yield (Metric Tons)	Depth (m)	M_0/W (10^{14} Nm/KT)	Ψ_∞/W (10^3 m^3/KT)
M-M QB	2	25	16.7	3.03
M&J (KQ01)	0.45	217	5.26	1.00
M-M (KQ01	0.45	217	9.87	1.79
M&J (KQ08)	0.15	10	5.26	2.51
M-M (KQ08)	0.15	10	31.7	5.76
RHS	0.068	5	2.25	0.34
M-M (RHS)	0.068	5	44.3	8.04
M-M (1 KT)	1000	300	8.00	1.45

Legend

M_0/W:
Moment scaled by yield.

Ψ_∞/W
Ψ_∞/W scaled by yield.

M-M QB:
Mueller-Murphy parameters in quarry blast explosive source (this report).

M&J (KQ01):
Source parameters of Shot KQ01 inferred by McEvilly and Johnson (1989).

M-M (KQ01):
Mueller-Murphy parameters for Shot KQ01.

M&J (KQ08):
Source parameters of Shot KQ08 inferred by McEvilly and Johnson (1989).

M-M (KQ08):
Mueller-Murphy parameters for Shot KQ08.

RHS:
Derived from elastic and cavity radii for shot in Reamer, Hinzen and Stump (1992).

M-M (RHS):
Mueller-Murphy parameters for shot in Reamer, Hinzen and Stump (1992).

M-M (1 KT):
Mueller-Murphy parameters for contained 1 KT bomb.

where r_c is the cavity radius, r_{el} is the elastic radius, c is the P wave speed and μ is the shear modulus. The source strengths in M&J, derived from moment tensor inversions, are reported directly. M&J shows the source strengths in their work and the Mueller-Murphy model have the same dependence on source depth (decreasing with scaled depth of burial), but that the scaled Ψ_∞ is about three times larger. This agrees with the results in Table 1, where we have tabulated Mueller-Murphy source strengths for shale at the same depths and yields as in M&J. We note that the values of the scaled Ψ_∞ for the source used in the quarry blast model reported here and the shallow M&J Shot KQ08 agree closely (although this is not the case for scaled moment). Whereas the Mueller-Murphy model gives larger source strengths than the M&J moment inversions, it yields smaller strengths than those in RH&S. This is due to smaller elastic and cavity radii in the Mueller-Murphy model than those inferred by RH&S. The strength of the source for our quarry blast study falls between the values reported by M&J and RH&S. The Mueller-Murphy model of the overburied 1 KT nuclear bomb has a source strength close to the value in M&J for their deep charge (KQ01, Table 1).

The calculations described in this report are not specific to any quarry. A site specific study that required accurate relative amplitudes between the nuclear test and the quarry blast would require that the explosion source function be more carefully specified. However, the referenced field studies indicate that the Mueller-Murphy source model is an appropriate source for the description of the seismic radiation from charges ranging from kilograms to kilotons.

2.3.2 Spall Model

Photographic observations of material thrown in the air by the explosions by Langefors and Kihlstrom (1963) show that typical velocities at which the material leaves the ground is in the range from 2 to 10 m/sec. These are also typical values for vertical ground velocities above nuclear explosions. Estimates of momentum of spalled rock we have obtained from a review of the blasting literature are consistent with model calculations conducted at S-CUBED in which the spall momentum of a contained explosion is roughly proportional to yield for shots detonated at scaled depths of burial between 50 and 200 m/KT$^{1/3}$. For hardrock, the corresponding momentum is 0.041×10^{12} N-sec/KT. Barker and Day (1990) used a tension crack model to describe numerical simulations of

nuclear events. The parameters of the model, vertical velocity, spall mass and momentum were consistent with observations. The parameters, scaled to 2 tons, are consistent with a block of material 20m on a side, ejected from a depth of 25 m at a velocity of 3.5 m/sec. These are reasonable values for the individual charges in a quarry blast as described above, and are what we used in the calculations for this report. A review of blasting literature reveals that the individual shots are generally conducted with scaled burdens of between 50 and 100 m /$KT^{1/3}$.

We compute the signal from the total quarry blast by linearly superposing the signals from individual holes. Several observations made during mine operations (Stump and Reinke, 1988, Reamer, *et al.* 1992, and Reamer and Hinzen, 1991) show that this approximation is valid. These authors also show that a point source representation of the cylindrical charges typically used in quarry blasts is valid.

2.4. Buried Explosion Source Model

In order to examine the hide-in-earthquake scenario, we have generated synthetic seismograms from explosions with equivalent yields of 0.1 KT and 1 KT. "Equivalent yield" refers to a tamped explosion with the given yield or a decoupled explosion of a larger yield reduced by decoupling to have an apparent yield (based on seismic signals) equal to the equivalent yield. Cavity decoupling has been investigated as a means of evading detection in a number of studies starting with Latter, *et al.* (1961). For a cavity decoupled explosion the equivalent yield is a function of the actual explosion yield and the size of the cavity. In Figure 6, we show the decoupling factor for an explosion in a salt cavity as a function of yield relative to the Latter yield for full decoupling. This figure is taken from Stevens, *et al* (1991) and extended to higher yields with some additional calculations. The decoupling factor is approximately 70 for a fully decoupled explosion, and decreases slowly up to a yield about a factor of 10 above the Latter yield, then decreases rapidly at higher yields. Also shown on the plot are measured decoupling factors from the Salmon/Sterling experiment, the Cowboy series of high explosive tests, and a recently published decoupling factor from a Soviet Azgir decoupled explosion (Adushkin, *et al*, 1992). The calculations shown in the figure agree quite well with the Salmon/Sterling experiment which showed a decoupling factor of 70 at an overdrive of 1.7 beyond the Latter yield,

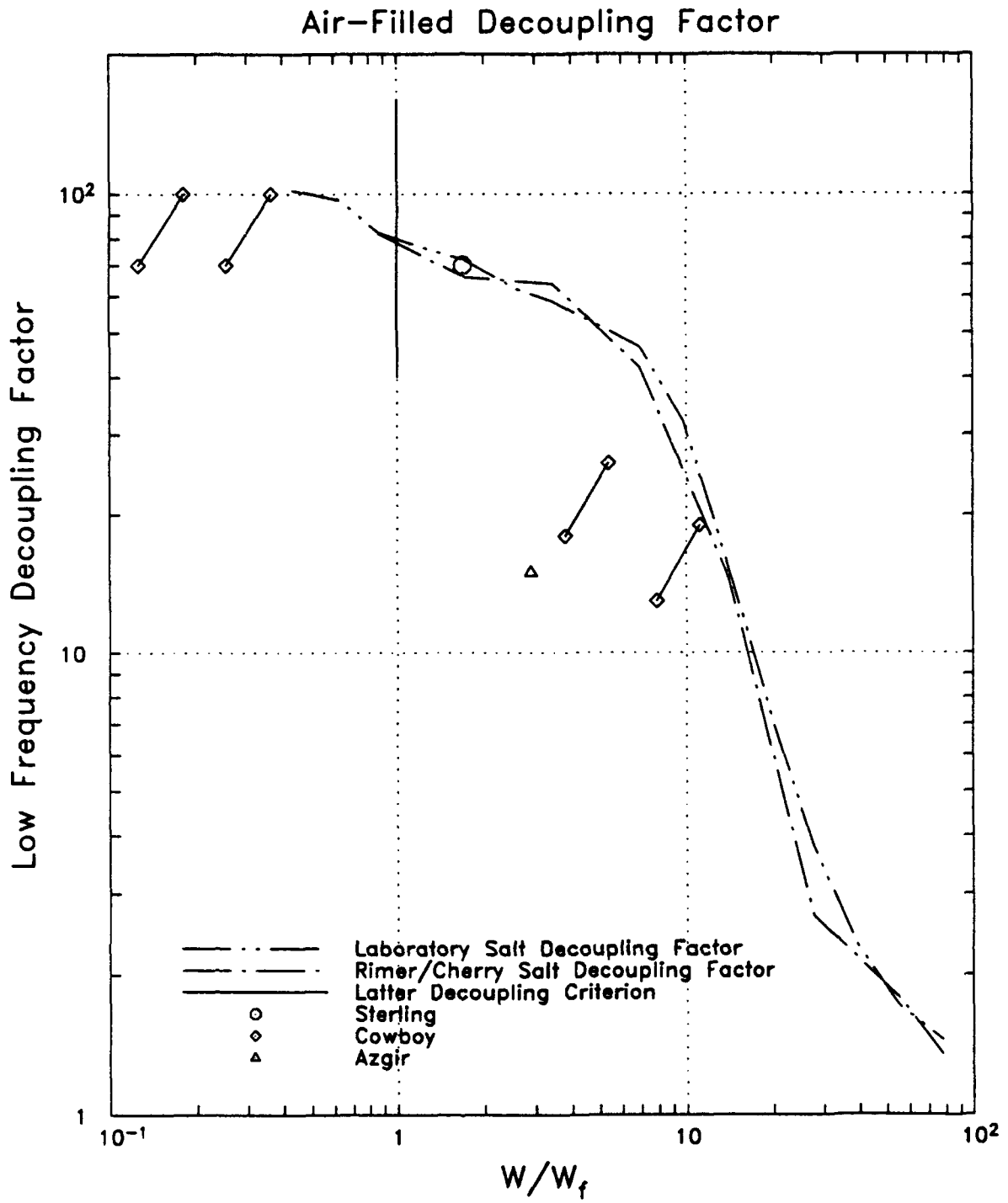

Figure 6. Decoupling factor for an explosion in an air-filled cavity in salt shown as a function of yield divided by the yield of a fully decoupled explosion from calculations by Stevens, *et al* (1991) for two different salt models. Also shown are data points for the Sterling explosion, the Cowboy HE tests, and the 3/29/76 Azgir test.

and are fairly consistent with the Cowboy tests (the data points with the line drawn between them correspond to the range of decoupling estimates for the overdriven Cowboy tests). The Azgir test however, appears to show an anomalously low decoupling factor of about 15 at an overdrive of 2.9 beyond the Latter yield.

It follows from Figure 6 that our 0.1 kiloton fully coupled simulation corresponds to a 7 kiloton fully decoupled explosion in a cavity with a radius of about 50 meters or, alternately, to somewhat smaller partially decoupled explosions in proportionally smaller cavities. A fully decoupled one kiloton explosion would generate signals 1/7 the size of our 0.1 kiloton fully coupled simulation.

2.5 Analysis of Synthetic Seismograms and Sonograms: Regional Phases

We have computed synthetic seismograms at a range of 1000 km using an earth model typical of the crust in central Asia (Table 2). A full wave integration procedure was used to calculate the Green's functions for the explosive and spall sources. A Green's function was calculated for every row of explosives to ensure that phase interference between rows was accurately computed. The calculations were done for the band from 0 to 5.0 Hz. To investigate the bomb-under-quarry scenario, we have also computed seismograms from tamped 0.1 KT and 1 KT explosions buried at 300 m. For the quarry blast simulation, the time interval between rows was 200 msec, starting with the row nearest the receiver. All charges within the rows were fired simultaneously.

We begin with the contributions to the seismograms due to movement of the spall mass. In Figures 7 and 8, we compare the vertical and radial ground motions from spall with four different combinations of initial height z_0 of the center of spall mass and angle θ_b that the initial trajectory makes with vertical (Figure 4). The radial motions are in the same direction as the horizontal component of spall movement. In the figures, the initial height is either zero or 10 m, and the angle is either zero (vertical) or 30^0. It can be seen that the effects of initial angle, and thus the effects of horizontal movement on both vertical and radial ground motions are small. However, the amplitudes for $z_o = 10$ are much

Table 2.
Earth Structure

Depth to Layer Bottom (m)	Layer Thickness (m)	P-Wave Velocity (m/sec)	S-Wave Velocity (m/sec)	Density (kg/m^3)	Shear Q
100.	100.	4692.	2332.	2574.	50.
1000.	900.	4692.	2332.	2574.	150.
6200.	5200.	6002.	3369.	2590.	500.
10200.	4000.	6298.	3535.	2698.	500.
20200.	10000.	6298.	3535.	2698.	500.
33200.	13000.	6650	3720.	2820.	500.
38200	5000.	6770.	3909.	2936.	500.
43200	5000.	6890.	3977.	2974.	500.
48200	5000.	8300.	4792.	3435.	500.
53200	5000.	8350.	4820.	3435.	500.
58200	5000.	8400.	4849.	3435.	500.
63200	5000.	8450.	4878.	3435.	500.
∞	∞	8500.	4907.	3435.	500.

larger than for $z_o = 0$. The increase is less pronounced at higher frequencies, as can be seen in the spectra in Figure 9 and in the signals highpass filtered above 2 Hz shown in Figure 10. To see why, consider the Fourier spectra of the spall force function (Equation (3)), which is plotted for $z_o = 0$ and 10 in Figure 11. The ratio of the peak spectral amplitudes is the ratio of impact velocities for the two cases (3.5 m/sec for $z_o = 0$ and 14.1 m/sec for $z_o = 10$). Note that as frequency tends to zero below 1.5 Hz, the spectrum for $z_o = 0$ approaches zero faster than for $z_o = 10$, so that the Rayleigh waves which dominate the broad band signals are much larger for $z_o = 10$. The highpass signals, however, scale roughly with the impact velocity. Another feature of the spectra for $z_o = 0$ is the scallop pattern with zeros at frequency intervals which are approximately $1/t_d$. The spectrum in Figure 10 for $z_o = 0$ and $\theta_b = 0$ shows the spectral holes clearly near 2 Hz and 3.4 Hz. The

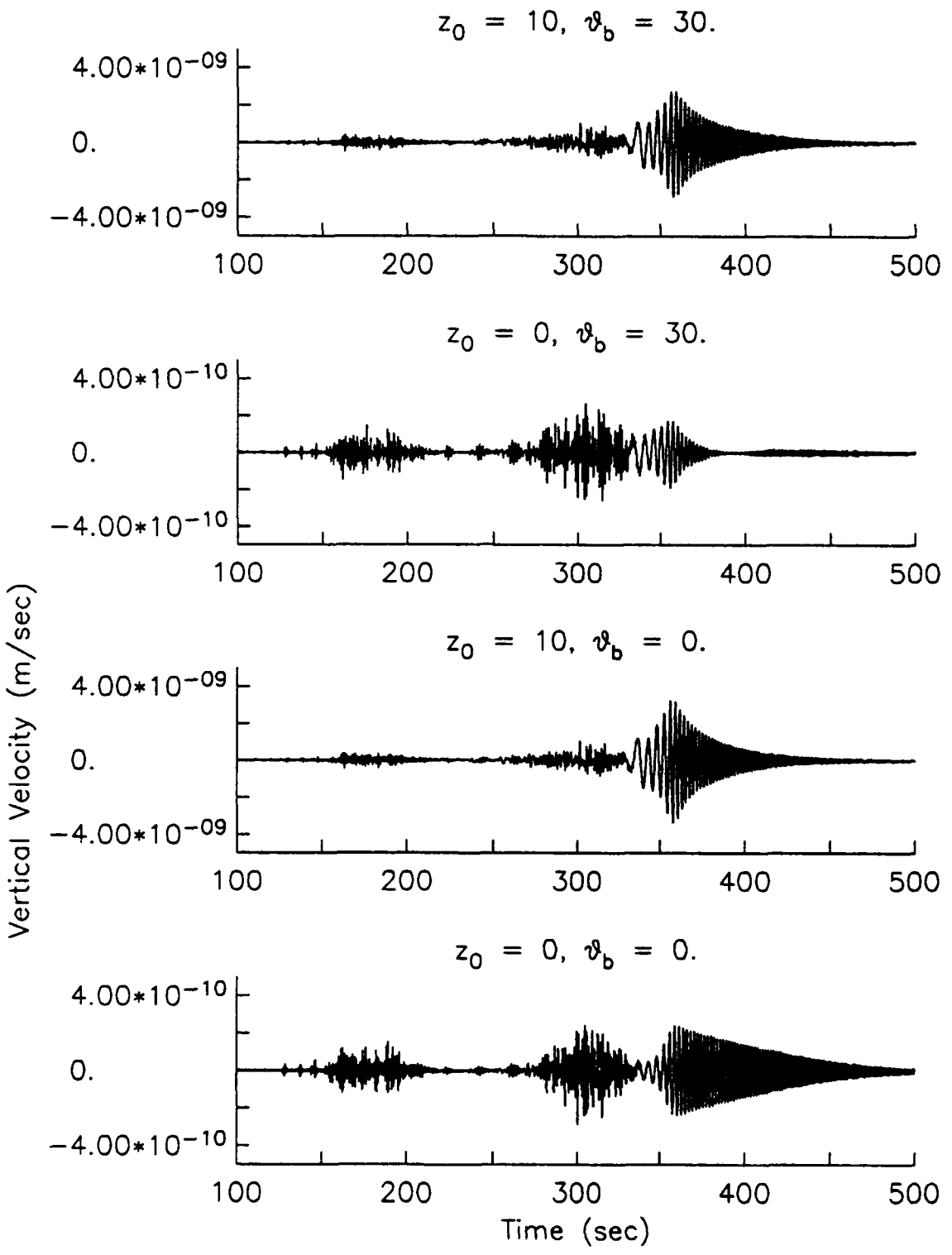

Figure 7. Contributions from the spall mechanism to regional synthetic vertical velocity seismograms at 1000 km (unfiltered) for values of initial height z_o and trajectory angle θ_b.

Spalls: Broadband Signals

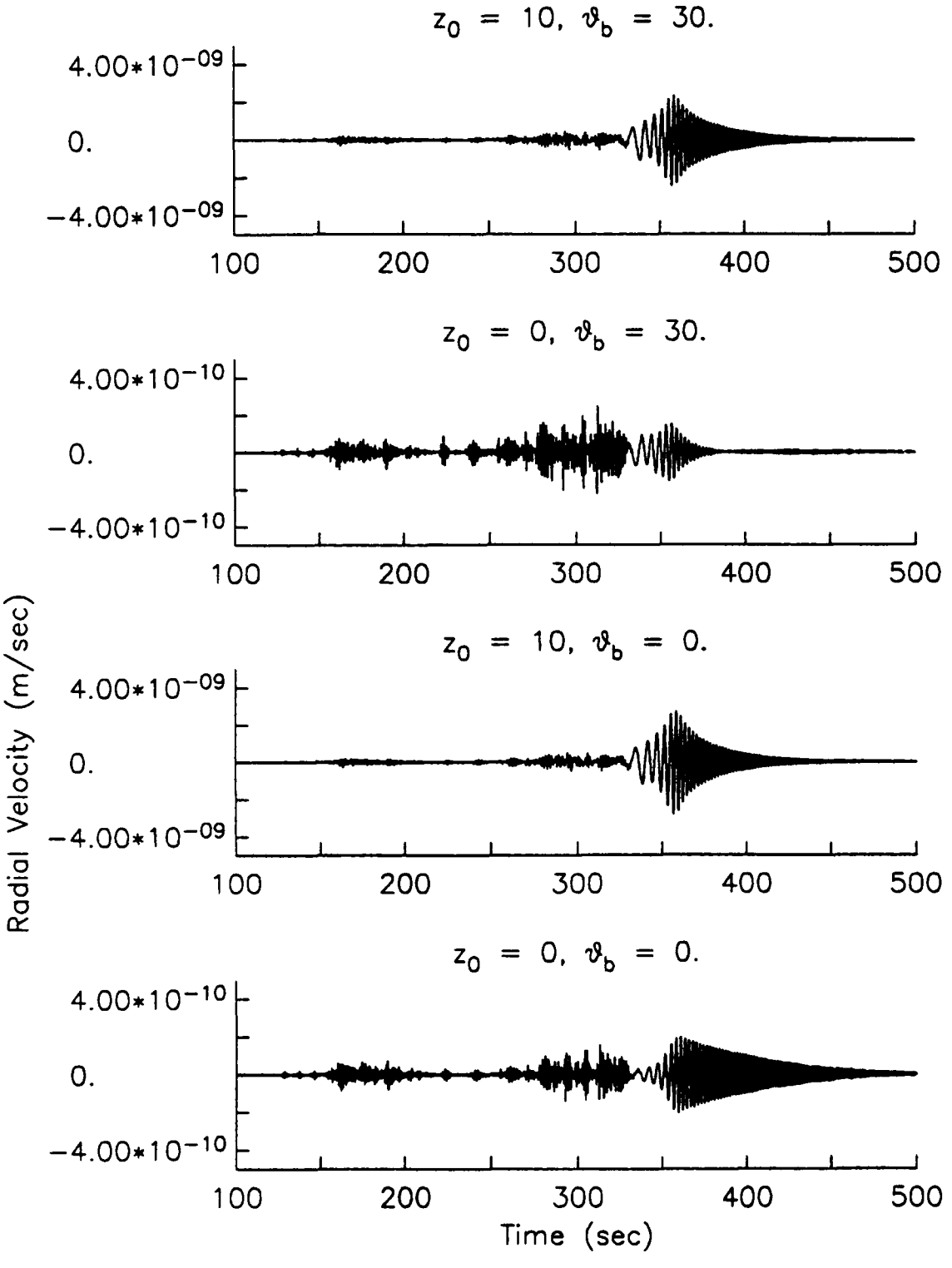

Figure 8. Contributions from the spall mechanism to regional synthetic vertical velocity seismograms at 1000 km (unfiltered) for values of initial height z_0 and trajectory angle θ_b (same as Figure 7, but for radial motions).

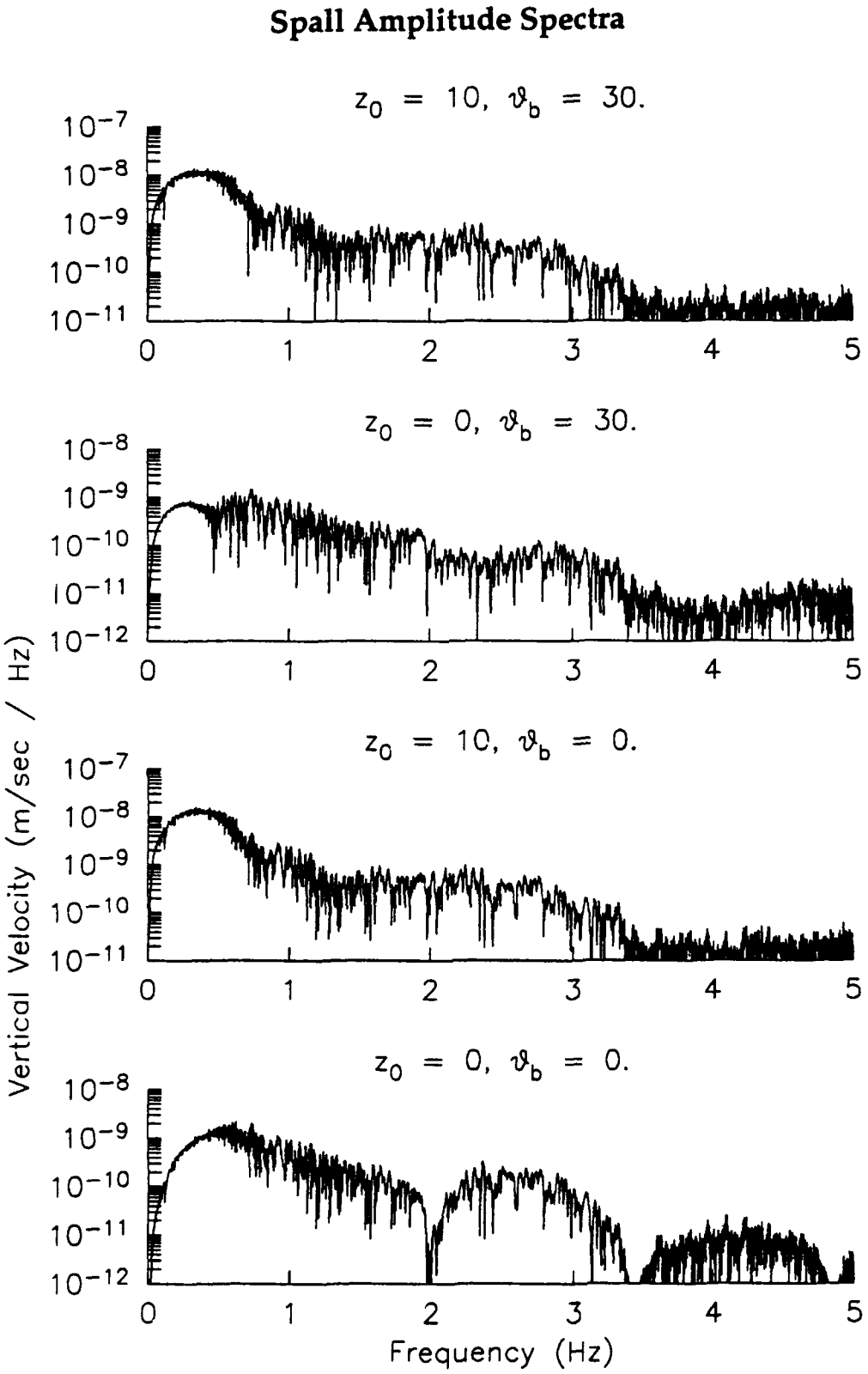

Figure 9. Contributions from the spall mechanism to regional synthetic vertical velocity spectra at 1000 km for values of initial height z_o and trajectory angle θ_b.

Spalls: Bandpass Filtered from 2.0 to 5.0 Hz

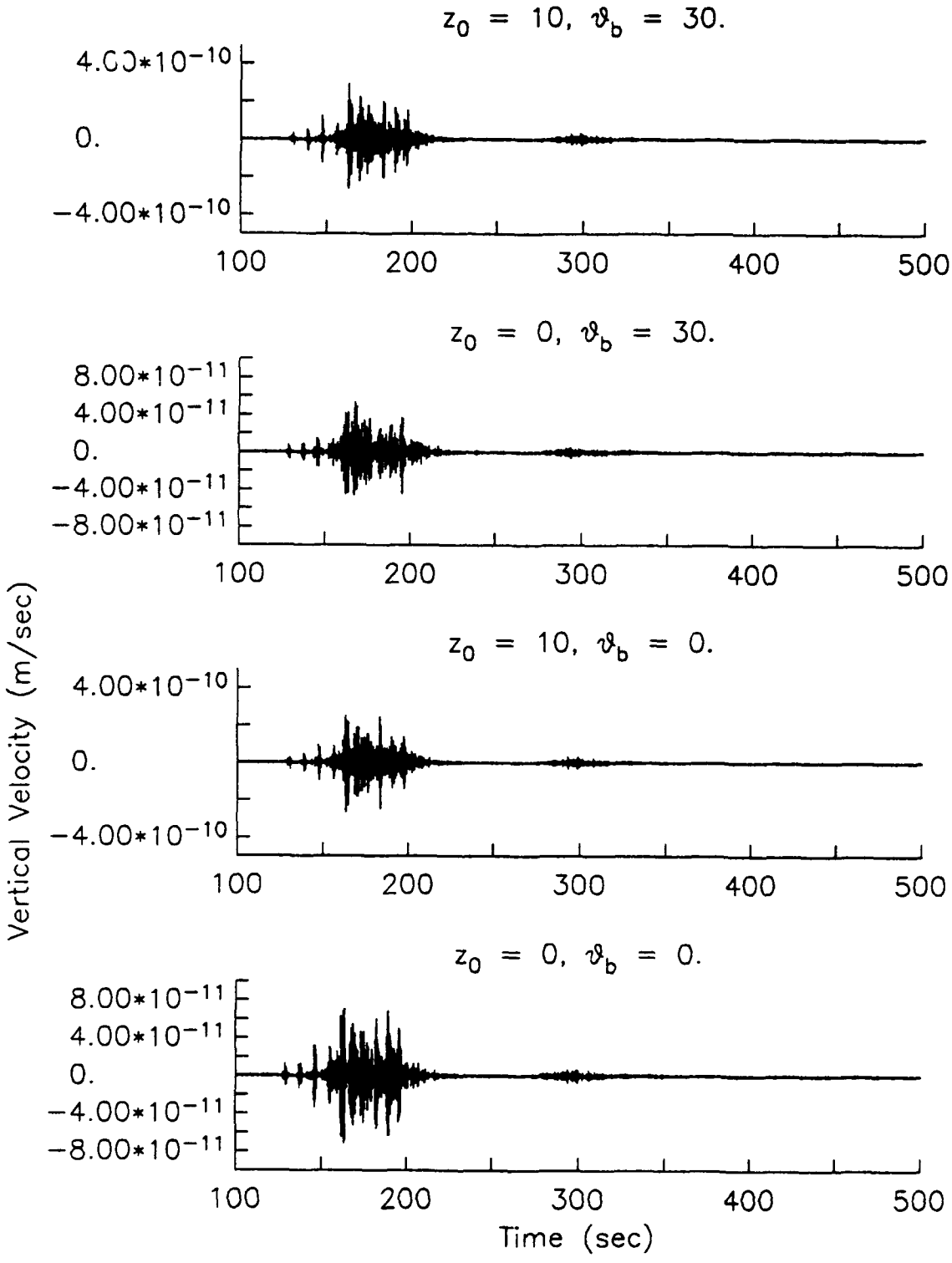

Figure 10. Contributions from the spall mechanism to regional synthetic vertical velocity seismograms at 1000 km (highpass filtered at 2 Hz) for values of initial height z_o = 0, 5 and 10 m and fixed trajectory angle θ_b.

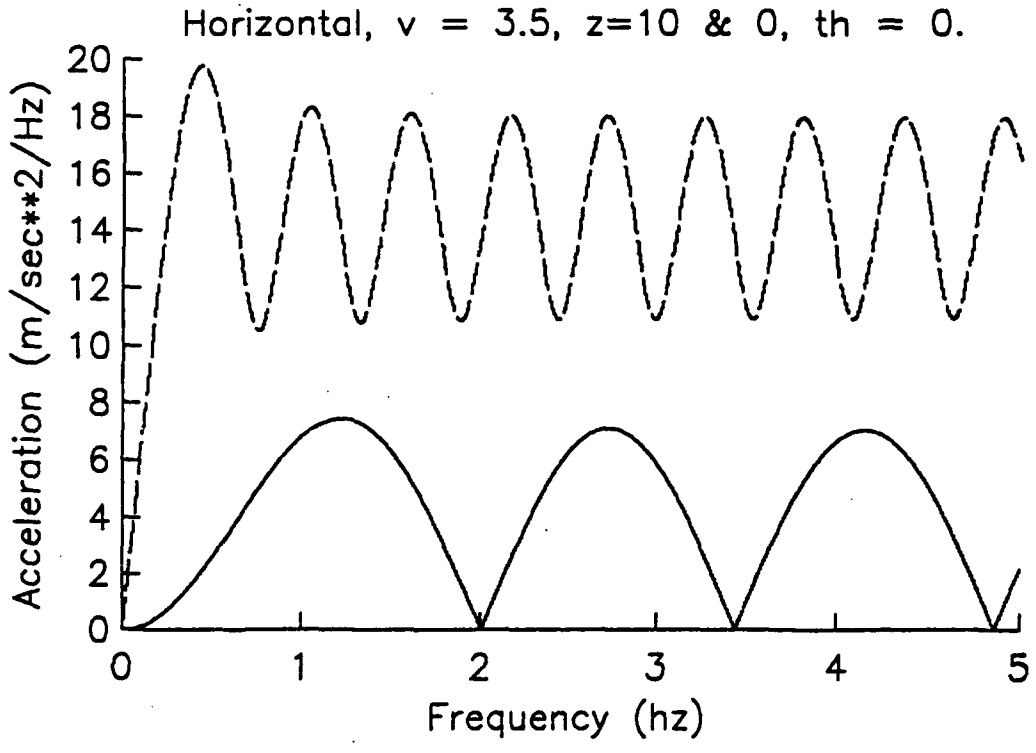

Figure 11. Spall source spectra for $\theta_b = 0$, with (top) $z_o = 10$, and (bottom) $z_o = 0$.

spectrum for $z_o = 0$ and $\theta_b = 30$ shows no holes due to the contribution from horizontal mass movement. The source spectrum for $z_o = 10$ in Figure 11 has no spectral holes. For the quarry with a bench the size of the one in the spall model considered here (30 m), the change in height of the spall mass is likely to be between 5 and 10 m. Calculations for this range of initial heights show that Rayleigh wave peak amplitudes are increased by about 5 to 10 times over those for no initial height, while higher frequency Pg and Lg peak amplitudes scale with the impact velocity.

The spall phase is induced by an explosive charge which, as discussed above, is modeled as a Mueller-Murphy source at a depth of 25 m. Figures 12 and 13 show the broadband and highpass filtered contributions from each shot hole due to the explosive charge, to the spall phase (with θ_o =30 and z_o = 10), and to the sum. The contributions from the charge and from spall are about the same. Note that the peak value on the highpass seismogram from the sum is not simply the sum of the peaks of the charge and spall, indicating different phase spectra.

Regional synthetic vertical and radial seismograms are shown in Figures 14 and 15 for the quarry blast simulation (20 x 25 shots at 0.002 KT), the tamped 1 KT explosion, the sum of the quarry blast and the tamped explosion, and from a single hole in the quarry blast. The quarry blast spall contributions were computed for $z_1 = 10$ m and $\theta_b = 30$. For these broadband velocity records, the signals are dominated by a normally dispersed Rayleigh wave. The Pg phase, arriving at about 160 seconds, and the Lg wave train, arriving between 275 and 375 seconds, can barely be seen. The peak motions from the quarry blast and the bomb are about the same.

Comparison of the peak amplitudes from the individual-shot seismogram with those from the quarry blast-alone seismogram show that the amplitude does not scale with the number of shots. This is due to the finite duration of the source. To see this, consider the expression for the spectrum of the ground motion from the quarry blast model. Denote by B_j^{exp} and B_j^{tc} the contraction of the moment tensor with the gradient of the propagation Green's function for the j^{th} explosion and tension crack source, respectively. The displacement spectrum for a distributed source with N_t shots detonated at times t_j is then

Broadband Signals

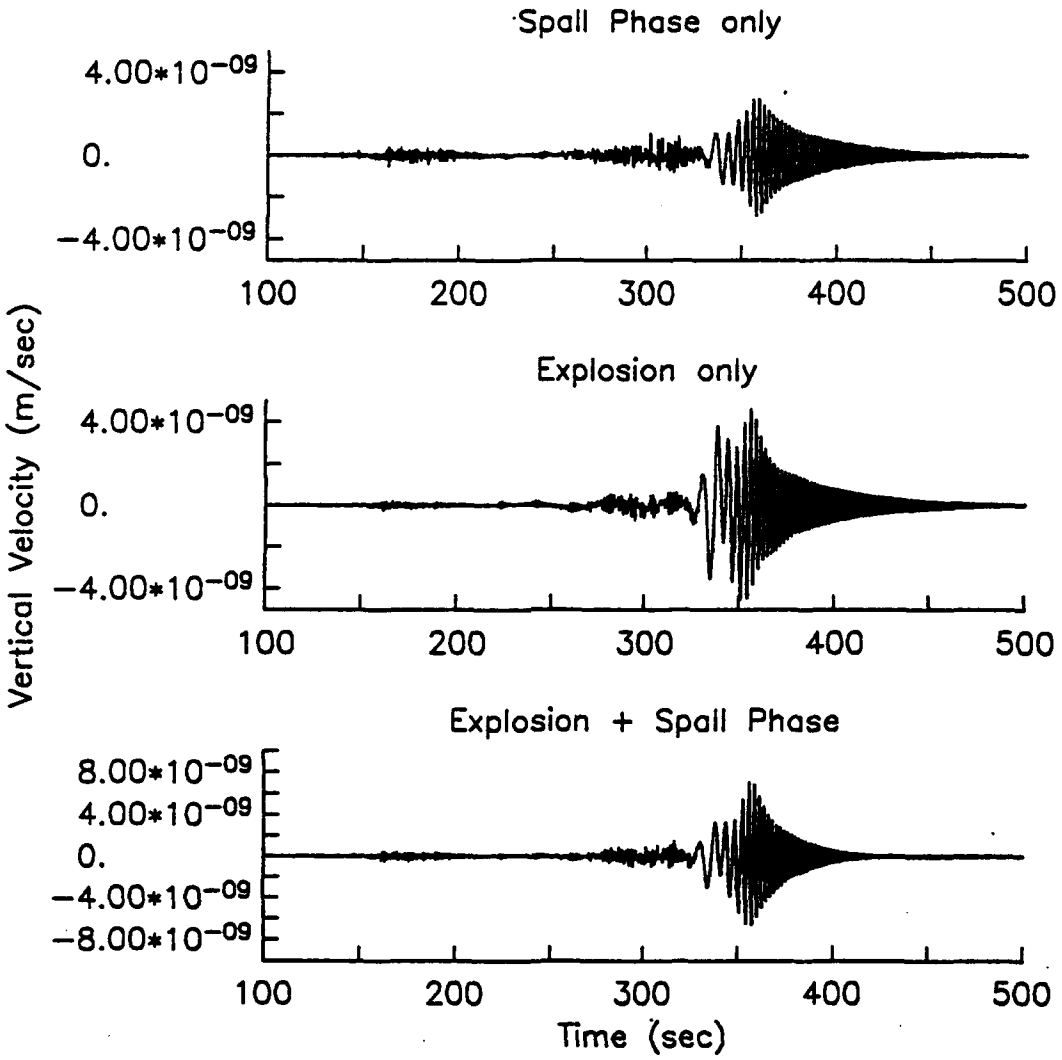

Figure 12. Regional broadband synthetic seismograms from a single shot: from top to bottom; the spall phase alone, the explosive charge alone and the sum of the spall phase and explosive charge.

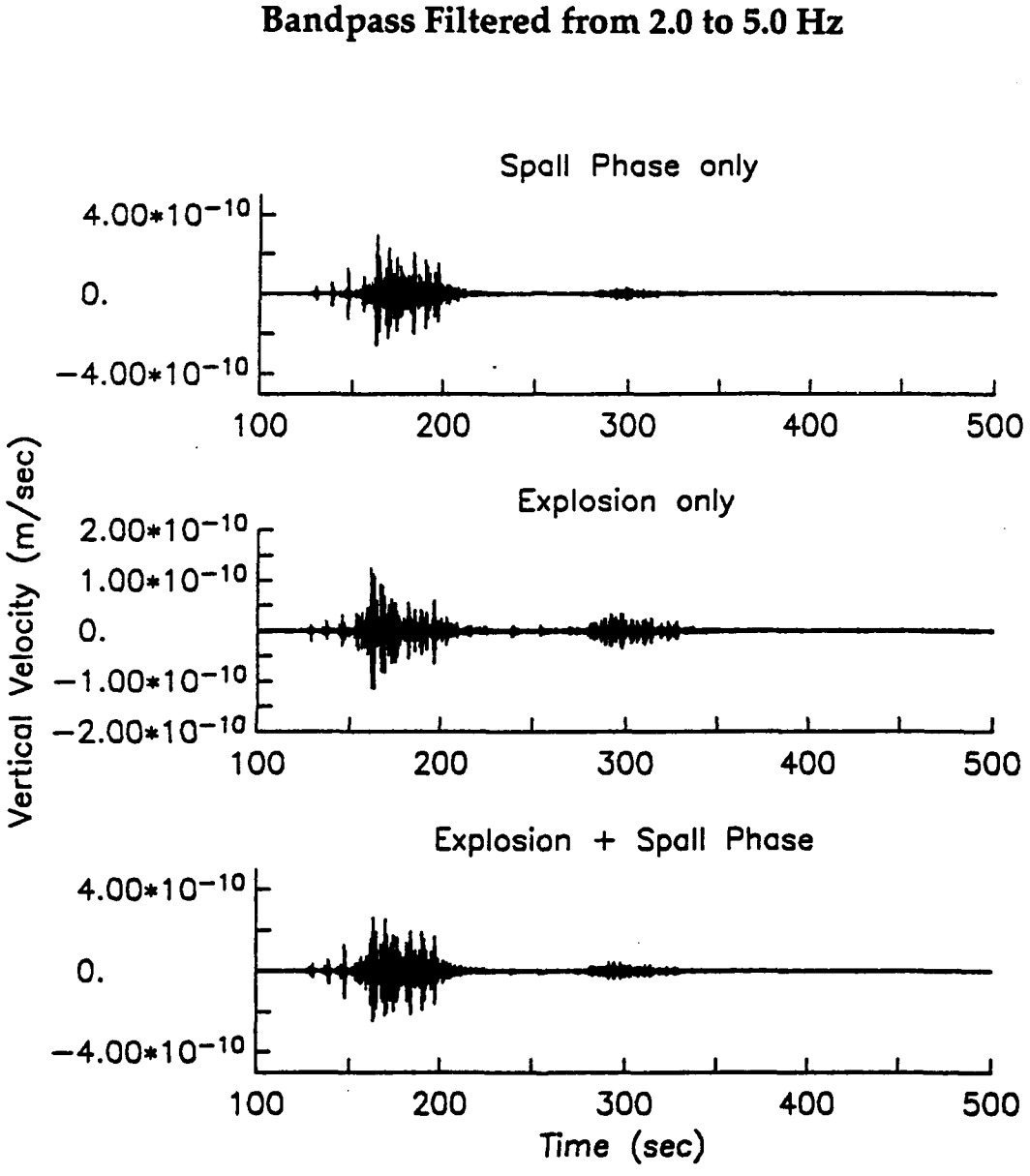

Figure 13. Regional narrow band synthetic seismograms (2.0 to 5.0 Hz) from a single shot: from top to bottom; the spall phase alone, the explosive charge alone and the sum of the spall phase and explosive charge.

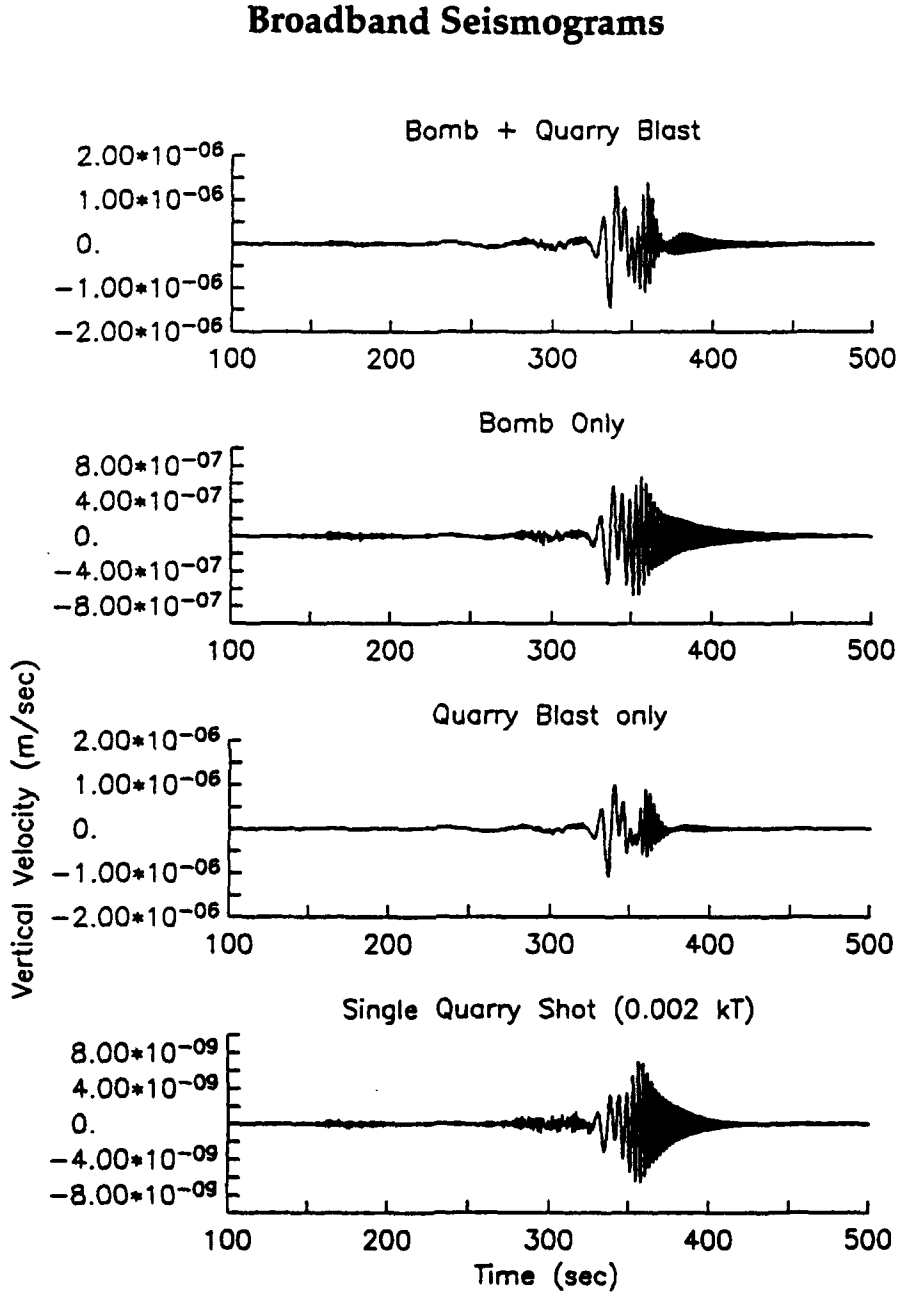

Figure 14. Regional synthetic vertical seismograms (unfiltered): from top to bottom; the sum of the quarry blast simulation plus the tamped 1 KT explosion, the tamped 1 KT explosion alone, the quarry blast simulation alone, a single hole in the quarry blast.

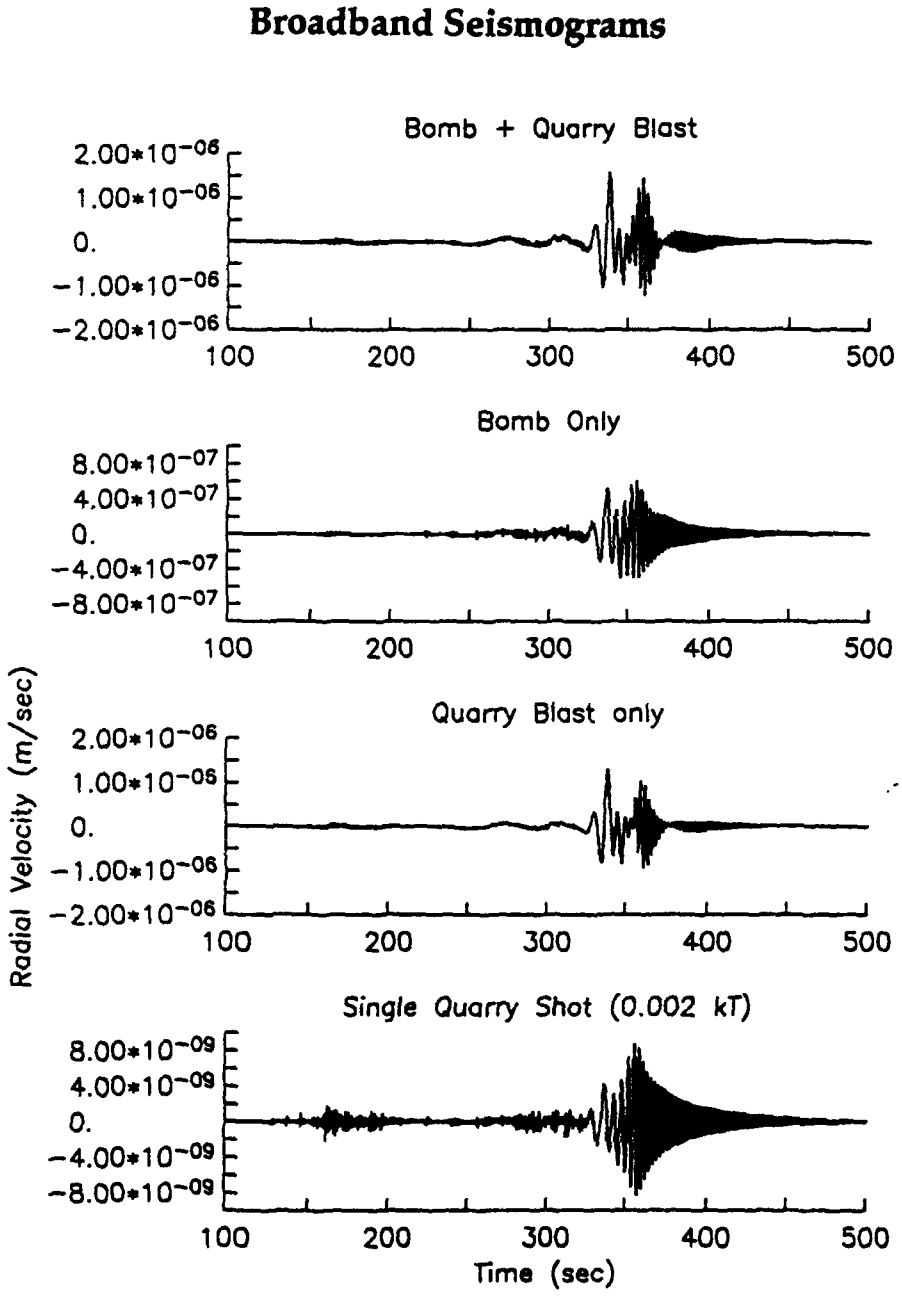

Figure 15. Regional synthetic radial seismograms (unfiltered): *from top to* bottom; the sum of the quarry blast simulation plus the tamped 1 KT explosion, the tamped 1 KT explosion alone, the quarry blast simulation alone, a single hole in the quarry blast (same as Figure 13, but for radial motions).

$$u(\omega) = \sum_{j=1}^{j=N} \left(B_j^{exp}(\omega) + B_j^{tc}(\omega) \right) e^{-i\omega t_j} \quad . \tag{4}$$

For the wavelengths of interest here, the Green's functions vary slowly over the quarry, and we can approximate the spectrum by

$$u(\omega) = \left(B^{exp}(\omega) + B^{tc}(\omega) \right) A(\omega) \quad . \tag{5}$$

where $A(\omega)$ is the "array response"

$$A(\omega) = \sum_{j=1}^{j=N_t} e^{-i\omega t_j} \quad . \tag{6}$$

Recall that we set the charges to detonate simultaneously within each row and fired the rows at $\delta t_s = 0.2$ sec intervals. If the number of rows is N_r and the number of shots per row is N_s, then the array response is

$$A(\omega) = N_s \sum_{j=1}^{j=N_r} e^{-i\omega j \delta t_s} \tag{7}$$

The sum in Equation (7) is in fact the digital Fourier transform of a boxcar function of duration $T = N_r\, \delta t_s$, given by a sin function with argument ωT. For the model discussed here, T = 4 sec. The array response is shown in Figure 18. At long periods, $A(\omega)$ scales linearly with the number of shots, that is, $A(\omega) \approx N_t = N_s N_r$, but decays at frequencies above about 1/2T, accounting for the scaling with the number of shots seen in Figure 16. Note also the scallops in the spectrum at frequency intervals of 1/T or 0.25 Hz. The scallops can also be seen in the spectra of the synthetic signals, as shown in Figure 19. Spectral holes caused by the source duration were observed in analyses of quarry blasts recorded at the NORESS array by Hedlin, *et al.* (1990). This effect has also been discussed by Smith (1992). The spectral shape in the bandwidth considered here does not depend strongly on the details of the firing pattern. The characteristic times of other features of the model such as delay times between and within rows and Lg propagation times across the source area are less than or equal to 0.2 sec, and so influence signals with frequencies above 5 Hz. In Figure 20, the array response is shown when a random variation with a standard deviation of 0.25 sec (a very large value) is added to the detonation time. Compare Figure 20 with

Bandpass Filtered from 2.0 to 5.0 Hz

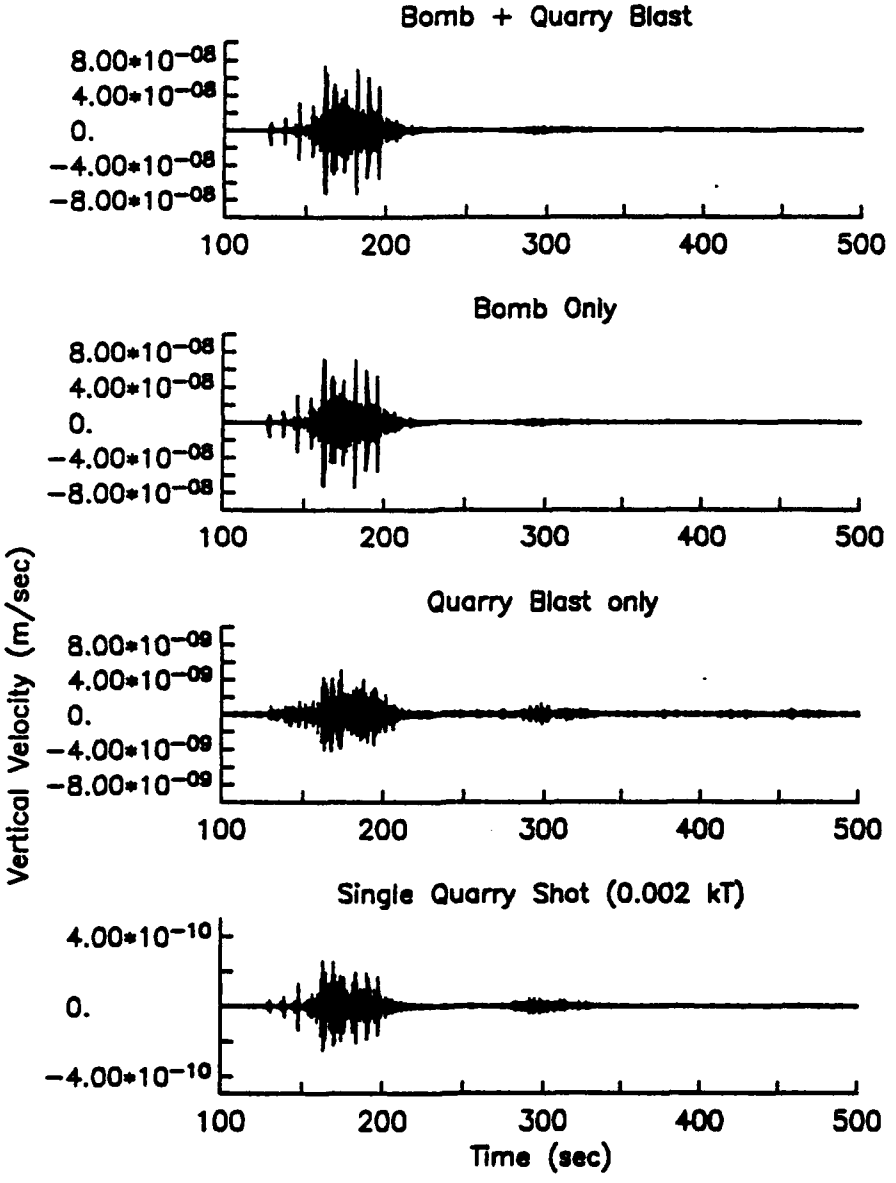

Figure 16. Regional narrow band vertical synthetic seismograms (2.0 to 5.0 Hz): from top to bottom; the sum of the quarry blast simulation plus the tamped 1 KT explosion, the tamped 1 KT explosion alone, the quarry blast simulation alone, a single hole in the quarry blast.

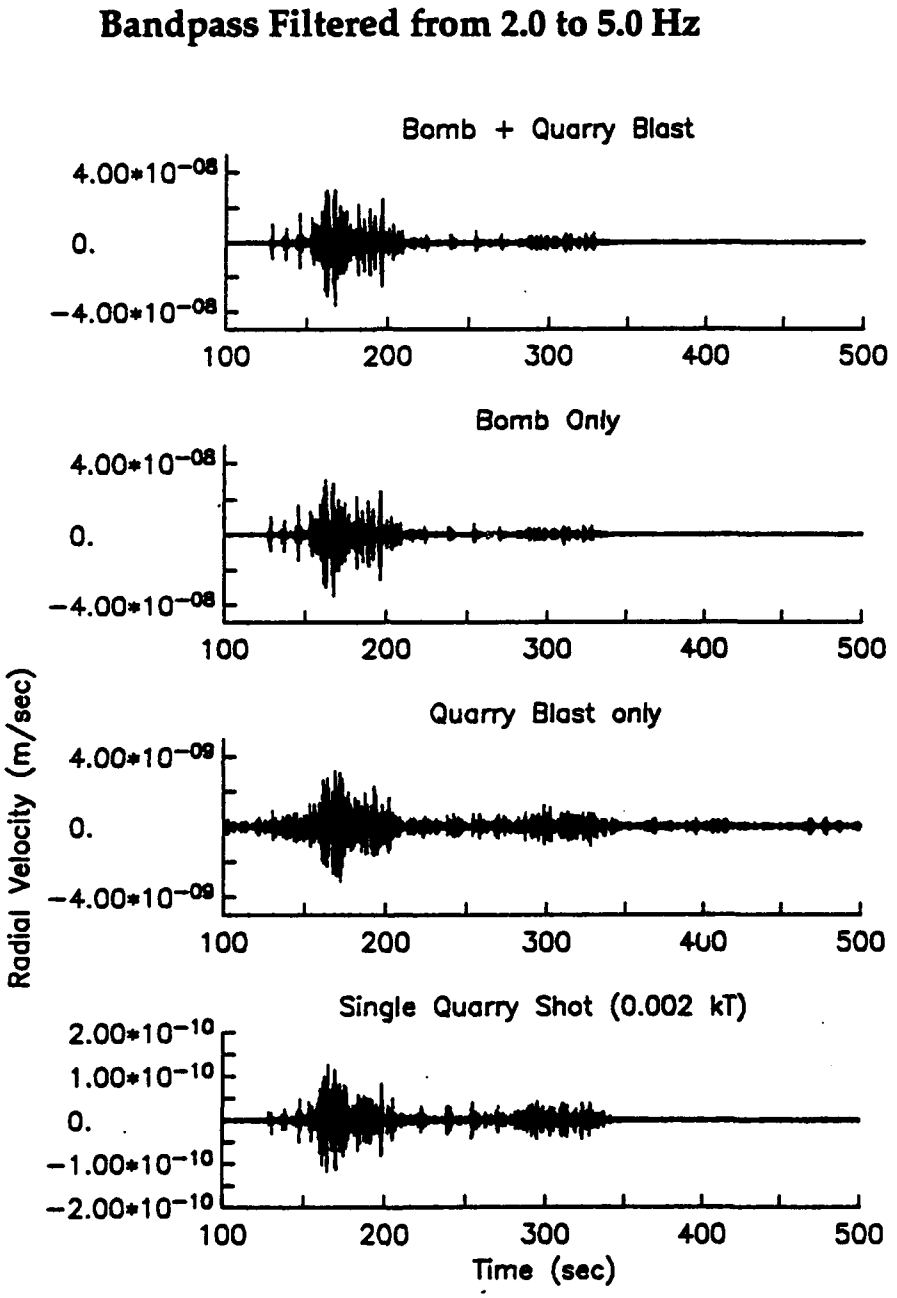

Figure 17. Regional narrow band radial synthetic seismograms (2.0 to 5.0 Hz): from top to bottom; the sum of the quarry blast simulation plus the tamped 1 KT explosion, the tamped 1 KT explosion alone, the quarry blast simulation alone, a single hole in the quarry blast (same as Figure 15, but for radial motions).

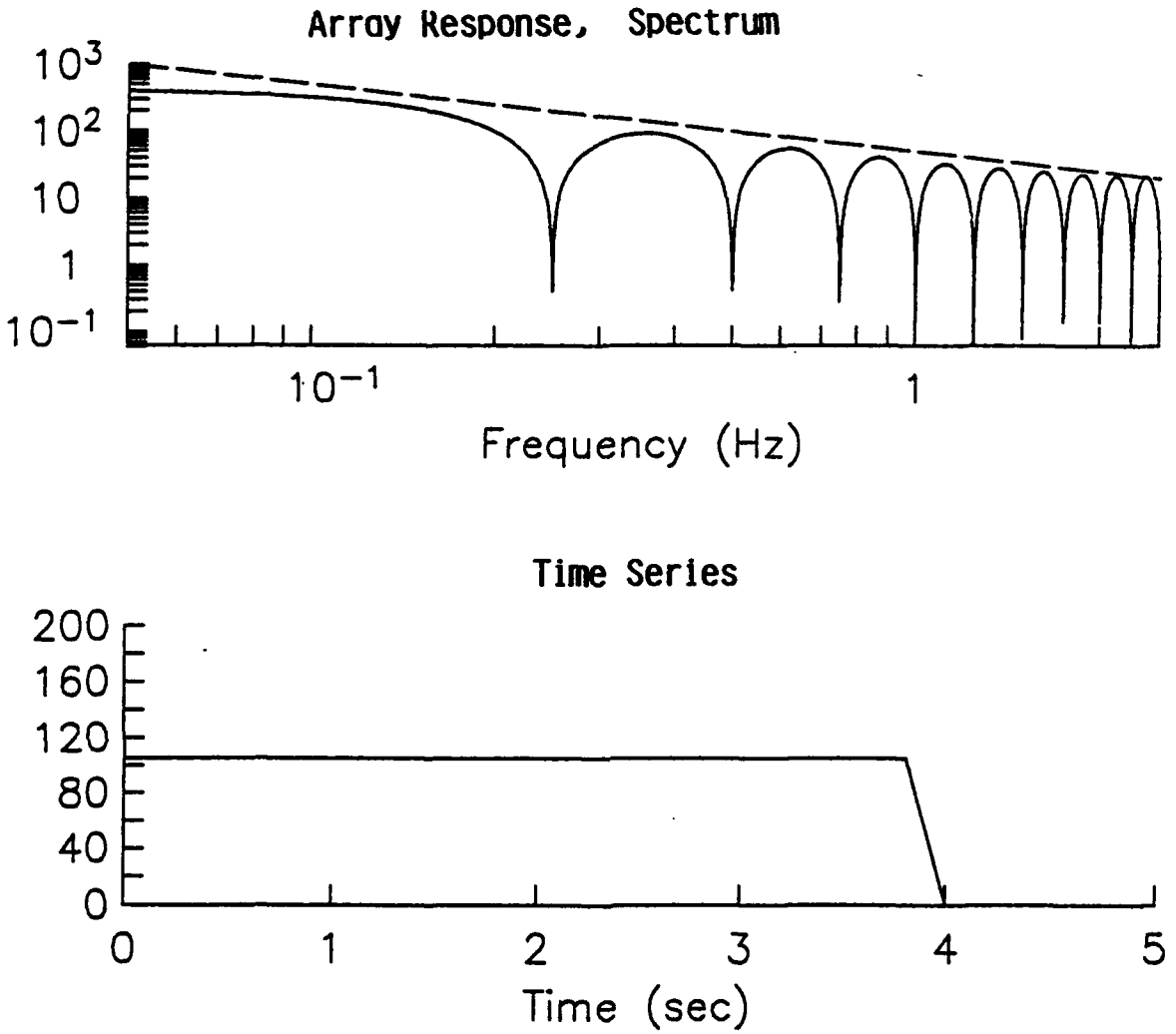

Figure 18. The response of the shot array for the 20x25 quarry: rows fired at 0.2 sec intervals. Dashed line on spectrum shows a line with slope f^{-1}.

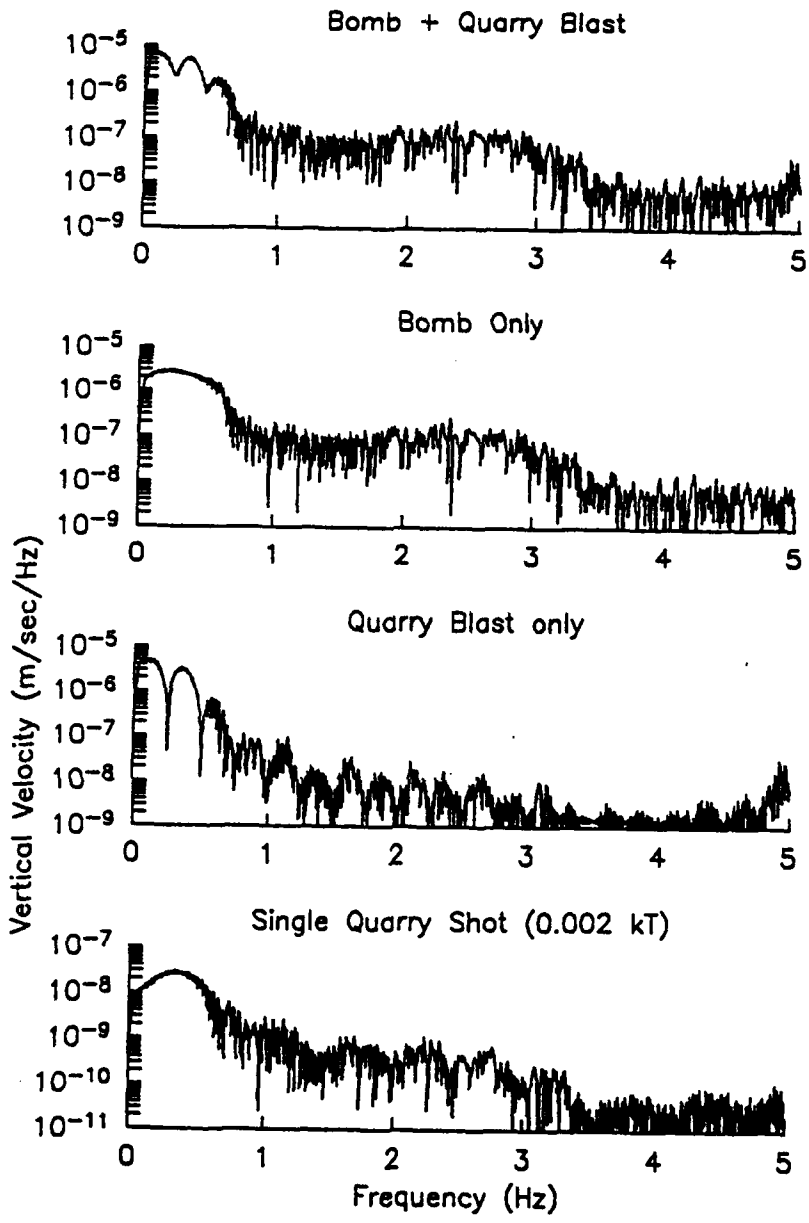

Figure 19. Vertical velocity spectra: from top to bottom; the sum of the quarry blast simulation plus the tamped 1 KT explosion, the tamped 1 KT explosion alone, the quarry blast simulation alone, a single hole in the quarry blast.

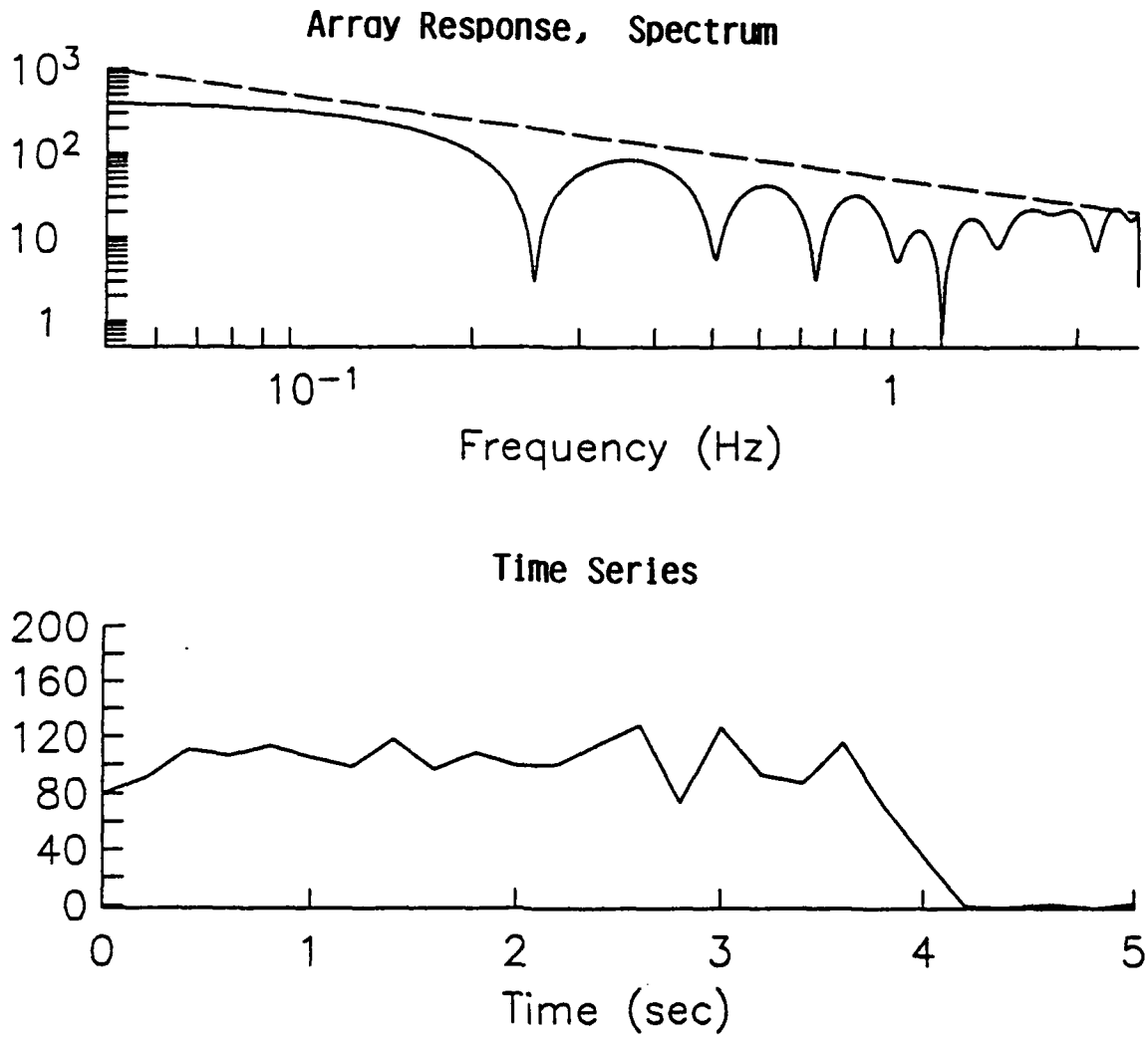

Figure 20. The response of the shot array for the 20x25 quarry: rows fired at 0.2 sec intervals with a 0.25 sec standard deviation in firing times. Dashed line on spectrum shows a line with slope f^{-1}.

Figure 3. The random variation weakens the spectral holes but the spectrum still begins to decay at about the same frequency and about the same rate. Synthetic seismograms computed with the array response with large deviations in firing times (i.e., Figure 20) are very similar to those in Figures 14 through 17.

The most important parameter for the bandwidth discussed here is the total source duration. In order to significantly enhance the signal amplitudes at Lg frequencies, say 2.5 Hz, the total duration of the source must shortened to less than about 0.2 sec (an unusual practice for a quarry blast with a total charge of 1 KT). In fact if the shots in our simulation were all fired simultaneously, the signal would look very much like the single-shot seismogram in Figure 5, multiplied by the number of shots (500). The spectrum in this case would have no scallops below about 6 Hz, corresponding to the time for the slowest Lg to cross the source array.

Figures 16 and 17 show the signals from Figures 14 and 15 filtered by a highpass filter with corner frequency 2 Hz. At the higher frequencies, the Pg phase dominates the records for both the quarry blast and the bomb. Peak amplitudes of Pg from the bomb are about 10 times larger than from the quarry blast, indicating that it would be difficult to hide the bomb in this frequency band.

A striking difference in the quarry blast and bomb signals is in the Pg spectra. In Figure 21, smoothed spectra of the Pg signals (windowed from before the Pn arrival to 250 seconds) from the two sources (the bomb and quarry blast discussed above) are compared. Also shown is the ratio of the smoothed spectra. At frequencies below about 0.4 Hz, the quarry blast amplitude is larger, but above that frequency the bomb Pg is larger. Above about 2.5 Hz, the bomb Pg exceeds the quarry blast Pg by a factor between 10 and 20. Lg spectra are shown in Figure 22. The time window for the Lg spectra was 250 to 350 seconds. The Lg spectra are similar, with the bomb amplitudes exceeding those of the quarry blast by a factor of 2 to 3 between 1.0 and 2.5 Hz.

The sonogram is a useful tool for viewing the relative excitation of seismic phases as functions of frequency. We show sonograms for the tamped 1 KT bomb, the 1 KT quarry blast model and their sum in Figures 23 through 25. On

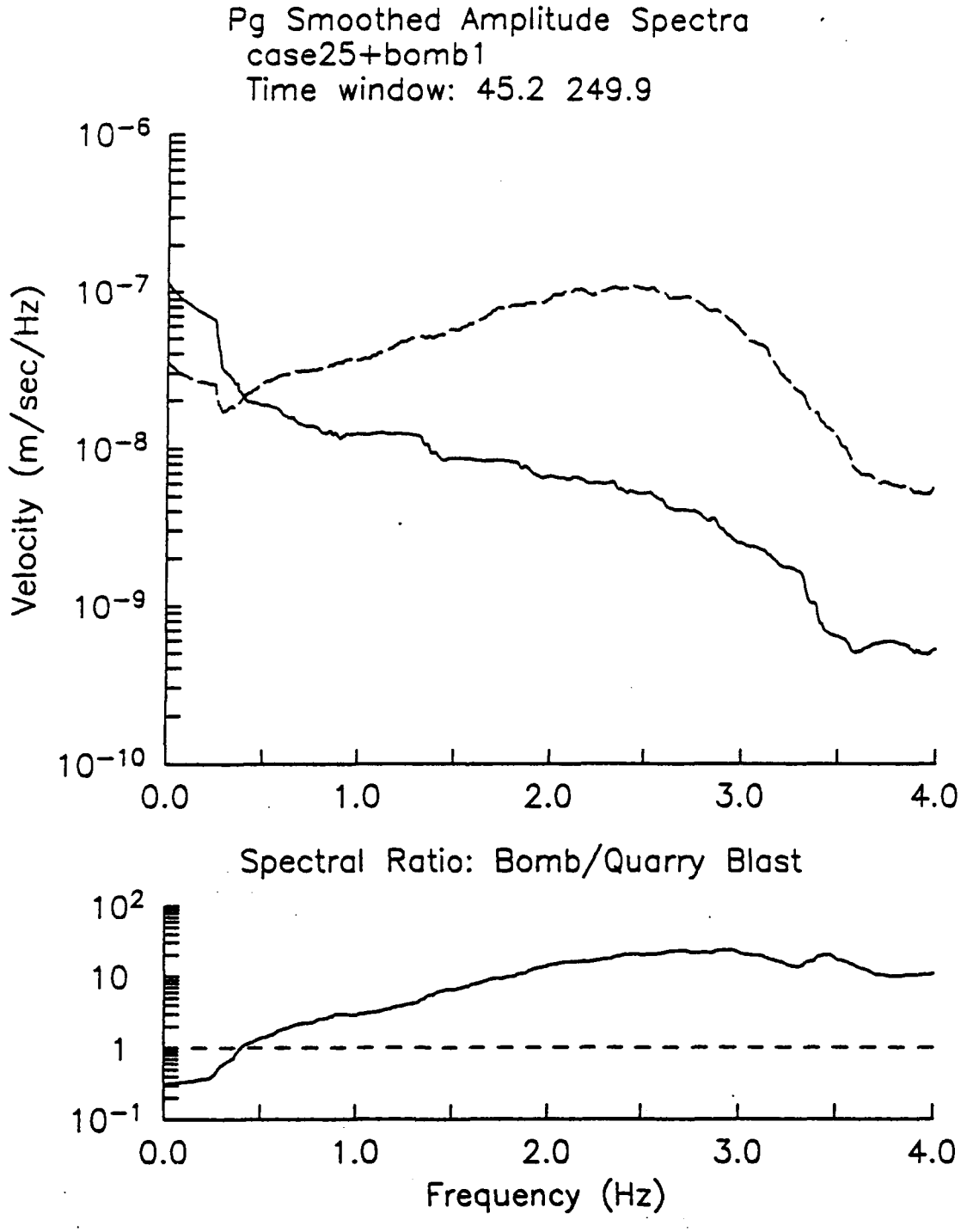

Figure 21. (top) Smoothed Pg spectra from the quarry blast (solid line) and the 1 KT bomb (dashed line). (bottom) Ratio of top spectra.

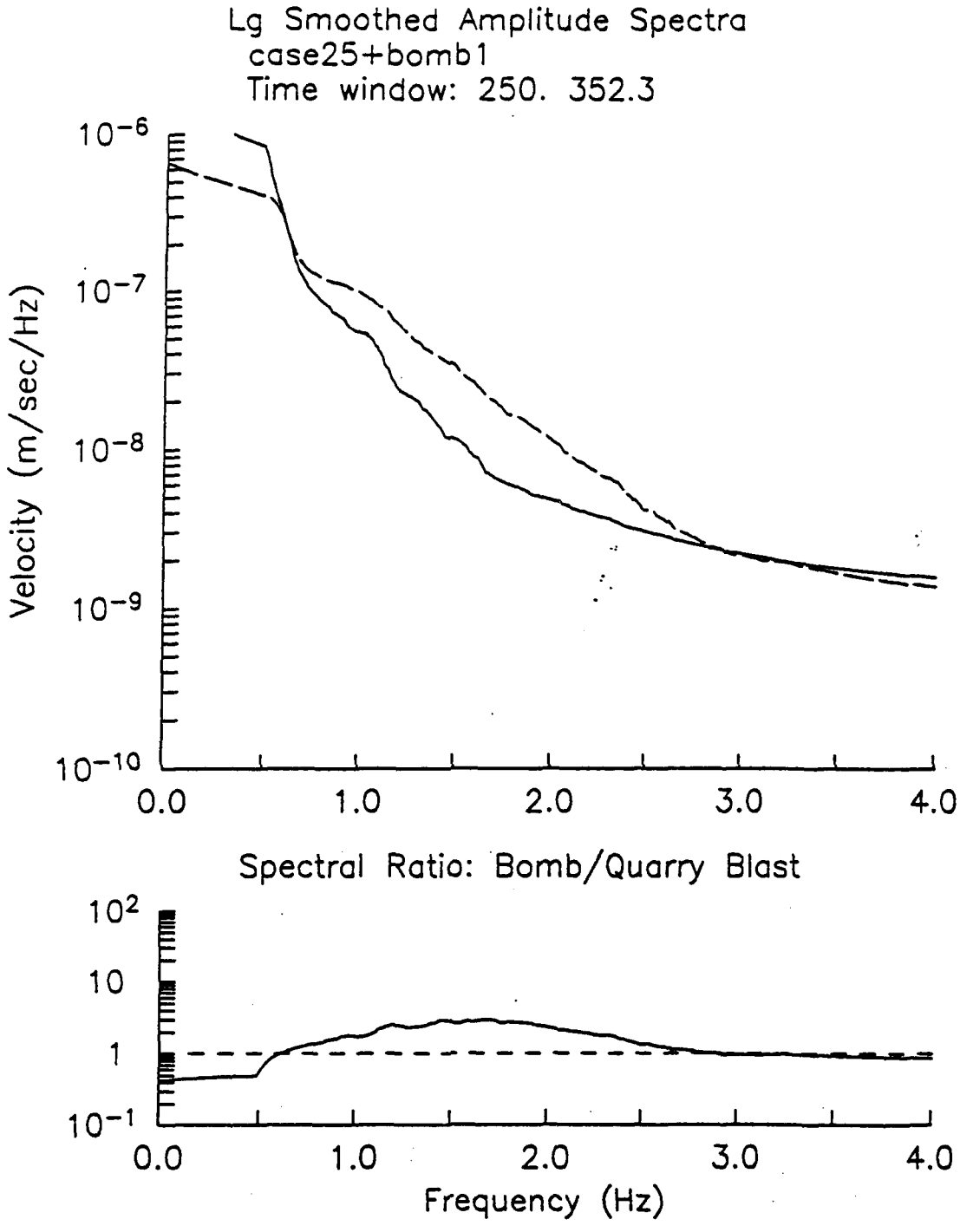

Figure 22. (top) Smoothed Lg spectra from the quarry blast (solid line) and the 1 KT bomb (dashed line). (bottom) Ratio of top spectra.

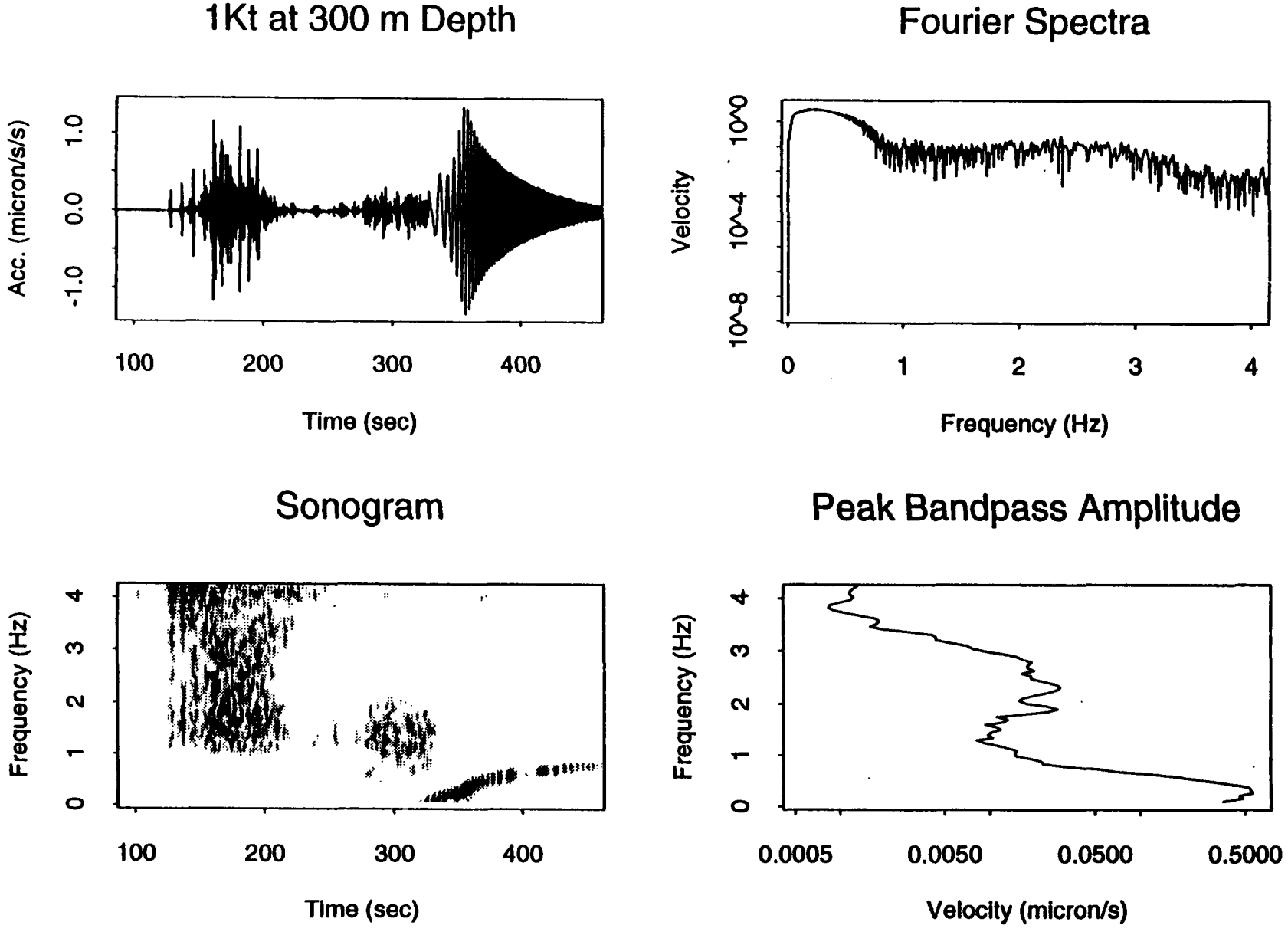

Figure 23. Four views of the vertical regional signals from the 1 KT bomb: (upper left) accelerogram; (upper right) acceleration spectrum; (lower left) sonogram; and (lower right) peak bandpass amplitude.

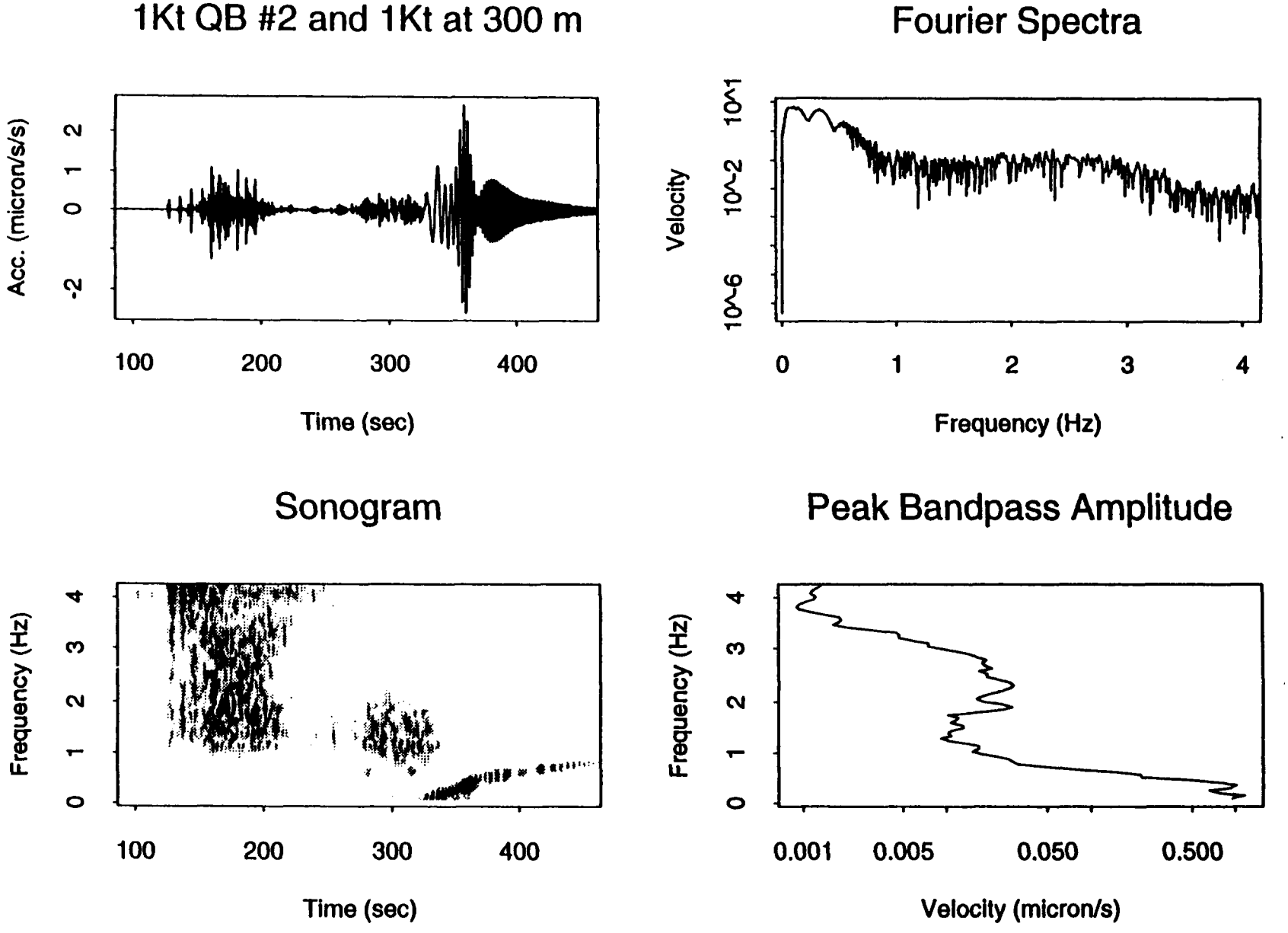

Figure 24. Four views of the vertical regional signals from the 1 KT quarry blast: (upper left) accelerogram; (upper right) acceleration spectrum; (lower left) sonogram; and (lower right) peak bandpass amplitude.

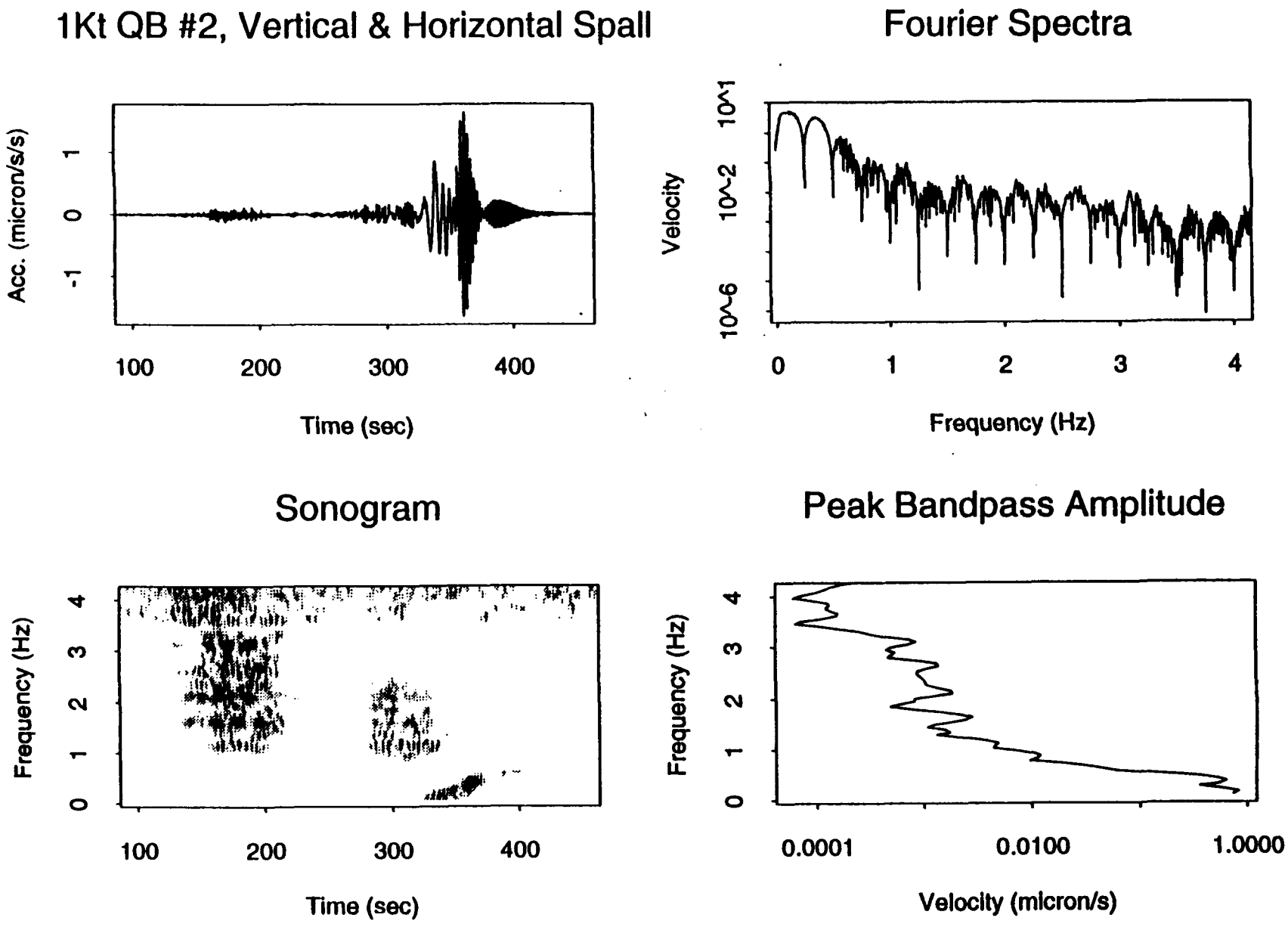

Figure 25. Four views of the vertical regional signals from the 1 KT bomb + 1 KT quarry blast: (upper left) accelerogram; (upper right) acceleration spectrum; (lower left) sonogram; and (lower right) peak bandpass amplitude.

each plot are the broad band seismograms (shown as accelerograms to emphasize the high frequencies), the Fourier spectrum of the entire signal, a spectrum formed from peak narrow band frequency amplitudes, and a sonogram. The sonograms have gain ranging which normalizes each band-pass signal to the peak at each frequency. Larger amplitudes appear darker on the figure. At low frequencies, the Rayleigh wave can be seen as the dispersed signals arriving near 330 seconds at the lowest frequency and is the dominant phase. Between 1 and 2 Hz, Pg (125 to 250 seconds) and Lg (250 to 350 seconds) are the largest phases, with Pg dominating above 2 Hz. The enhancement of Pg from the bomb at high frequencies is evident on both the sonograms and on the accelerograms,

A comparable analysis for a much smaller tamped bomb is summarized in Figures 26 and 27. In this case the bomb, with a yield of 0.1 KT, is added to the same 1 KT quarry blast. At this lower yield, the bomb is masked by the quarry blast in the accelerogram. Note, however, that the spectral scallops from the quarry blast are still apparent at low frequencies.

For a plane layered model, the explosive sources and the vertical movement of the spall mass would generate no SH waves, whereas lateral movement would produce an SH radiation pattern proportional to the sine of the angle from the direction of movement. In reality, SH waves are generated by the explosions. Without an accurate scattering model, one cannot estimate the relative contributions to SH motions of lateral movement and scattering from the explosive and vertical movements.

It is interesting to note that the spall source contributes to the bandwidth studied here because of the characteristic time for the burden to fly up and return. Barker and Day (1990) show that the spall model has a narrow-band source spectrum peaked at a frequency which is the inverse dwell time of the material in the air. Recall from above that typical throw velocities for quarries are 2 to 10 m/sec, for which the dwell times are 0.2 to 2.0 seconds. Spectral peaks for the spall would occur between 0.5 and 5 Hz, which is in the regional seismic band.

Bandpass Filtered from 2.0 to 5.0 Hz

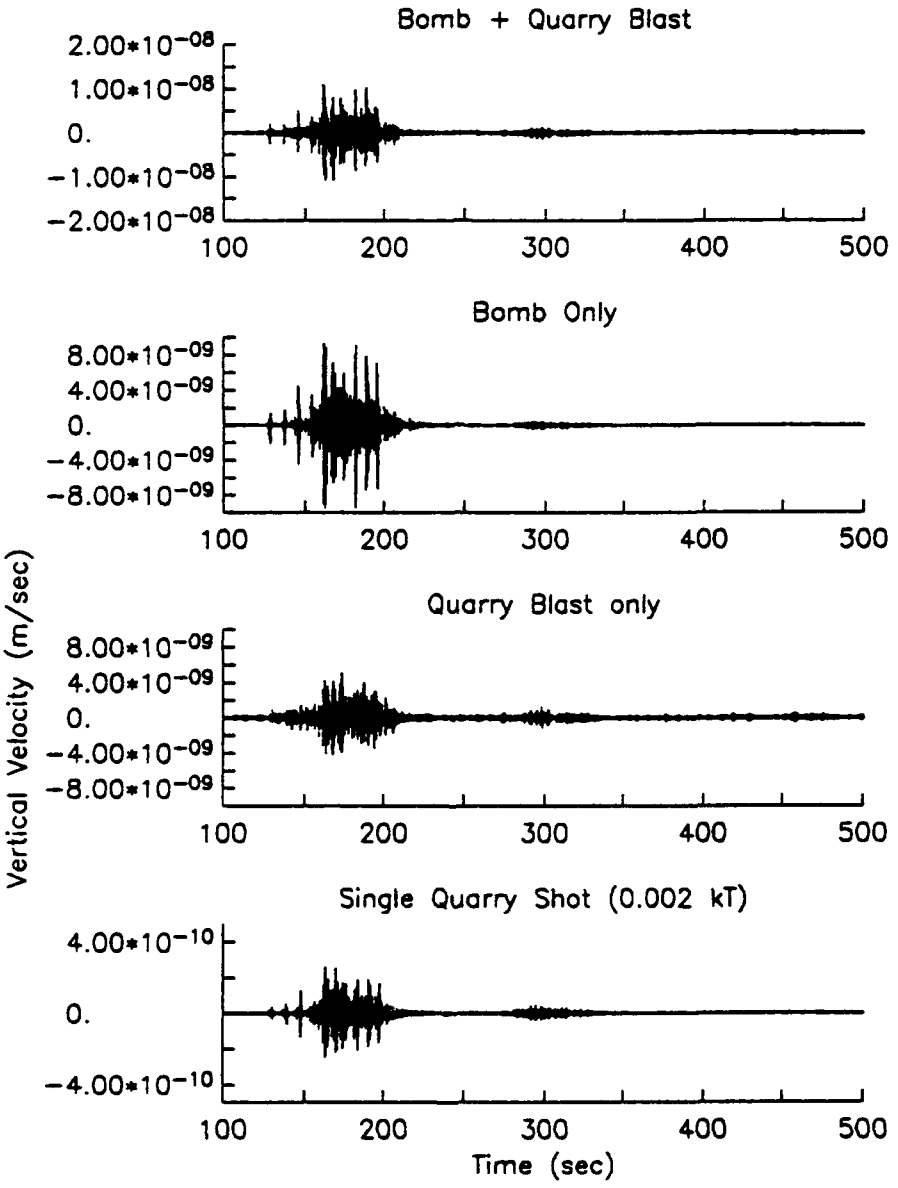

Figure 26. Regional narrow band vertical synthetic seismograms (2.0 to 5.0 Hz): from top to bottom; the sum of the quarry blast simulation plus the tamped 0.1 KT explosion, the tamped 0.1 KT explosion alone, the quarry blast simulation alone, a single hole in the quarry blast.

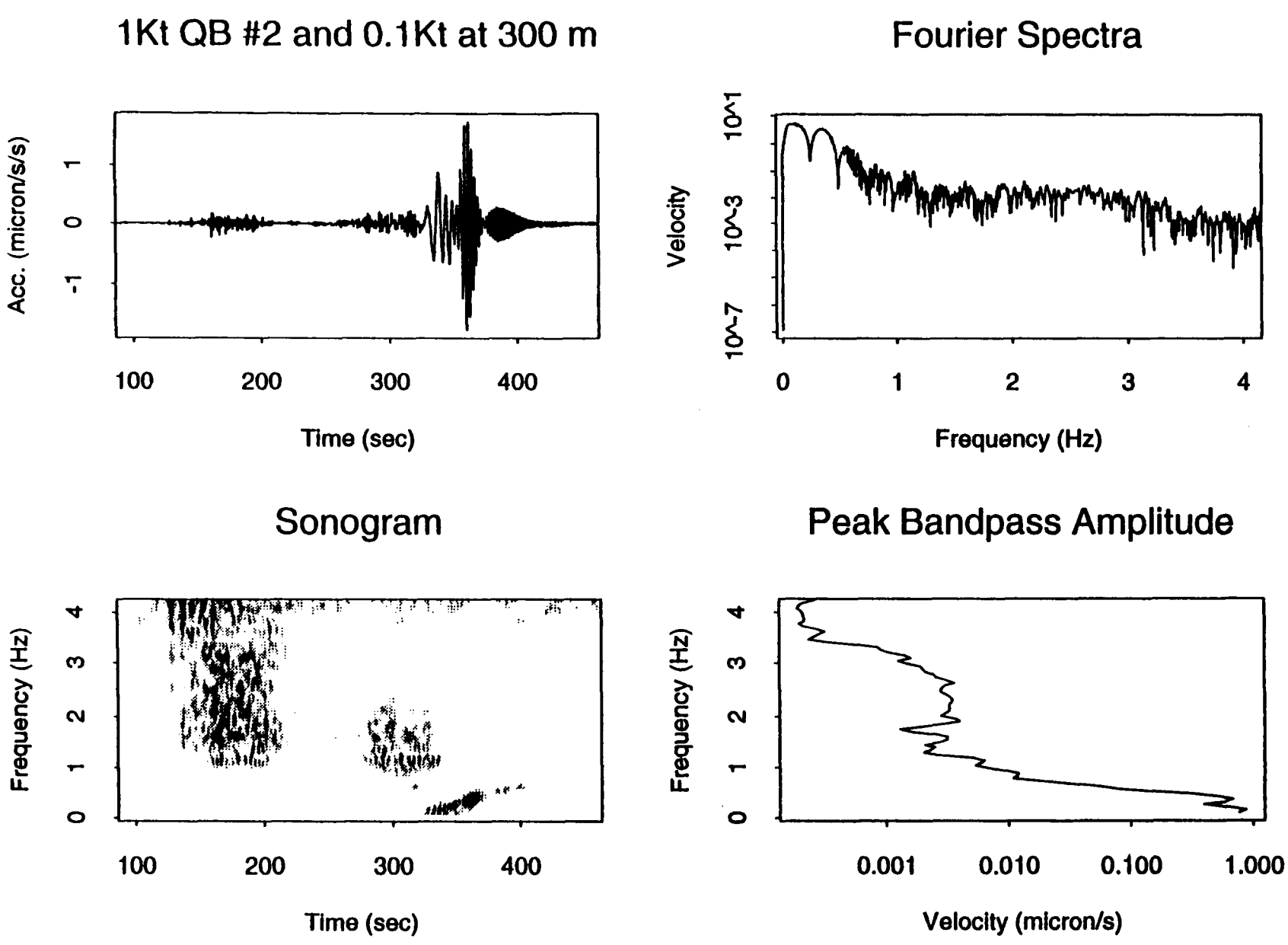

Figure 27. Four views of the vertical regional signals from the 0.1 KT bomb + 1 KT quarry blast: (upper left) accelerogram; (uper right) acceleration spectrum; ()lower left) sonogram; and (lower right) peak bandpass amplitude.

The low frequency Rg phase is not visible in the 2 to 2.5 Hz bandpass of the synthetic seismograms discussed above. In Figure 28, we have broadened the band to 0.75 to 2.5 Hz. The Rg phase is now apparent in the figure. Note the phase interference in the quarry blast simulation caused by a spectral hole (due to source duration) which has diminished the signal at the phase velocity associated with the frequency of the hole.

To check the amplitudes from the synthetic signals, we have computed the local magnitude M_L. After convolving the records in Figure 16 with a Wood-Anderson instrument response, we find that the peak amplitude of Pg from the bomb is about 0.15 mm at a distance of 1000 km (Figure 29). Using the distance correction curves (extrapolated to 1000 km) in Richter (1958), we find that M_L = 4.6, a reasonable value for a 1 KT bomb. M_L computed from the Lg phase for the bomb and for the quarry blast alone is 4.1 in both cases. Based on Isrealson and Carter (1991) , values of M_L for 0.1 KT Scandinavian quarry blasts fall in the range from 2.0 to 2.7, and a 1 KT quarry blast in Scandinavia might produce an M_L as large as 3.7. We have used here the attenuation rule appropriate for southern California (Richter, 1958) to estimate synthetic M_L but our earth structure was a high-Q shield structure. The M_L difference, 4.1 - 3.7 = 0.4, is consistent with an underestimation by the western U.S. attenuation law by a factor of 3 in amplitude at a distance of 1000 km.

2.6 Analysis of Synthetic Seismograms: Teleseismic Phases

Using the methods described in Barker and Day (1990), we computed teleseismic P waves for the quarry blast and bomb model discussed above at a range of 25°. In this calculation, we computed the geometric spreading rate from the Herrin travel time tables (assuming the upper mantle and crust did not disperse the signals), computed an anelastic attenuation based on a t^* of 0.7, and used a free surface receiver function of 1.8. The time series were convolved with a short period SRO instrument response. Since the scaled depth of burial of the 1 KT bomb was large (300), we assumed that the interaction with the free surface above the source was linear (no spall). The synthetic records are shown in Figure 30. As with the regional signals discussed above, the signal from the 1 KT bomb is bigger than the quarry blast signal, in this case by a factor of about 2.5. Unlike the regional case, the teleseismic quarry blast signal from the explosive

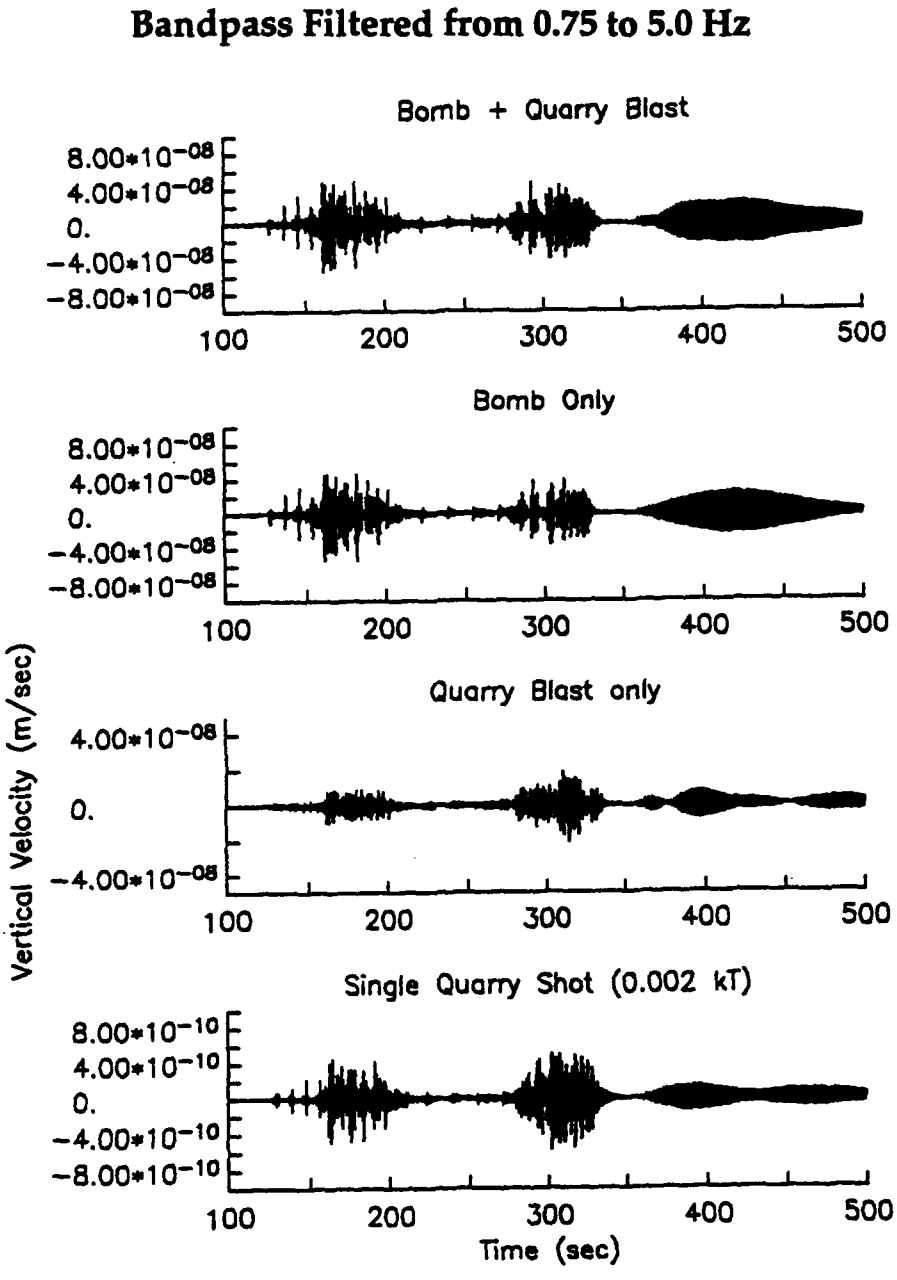

Figure 28. Regional narrow band synthetic seismograms (0.75 to 5.0 Hz): from top to bottom; the sum of the quarry blast simulation plus the tamped 1 KT explosion, the tamped 1 KT explosion alone, the quarry blast simulation alone, a single hole in the quarry blast.

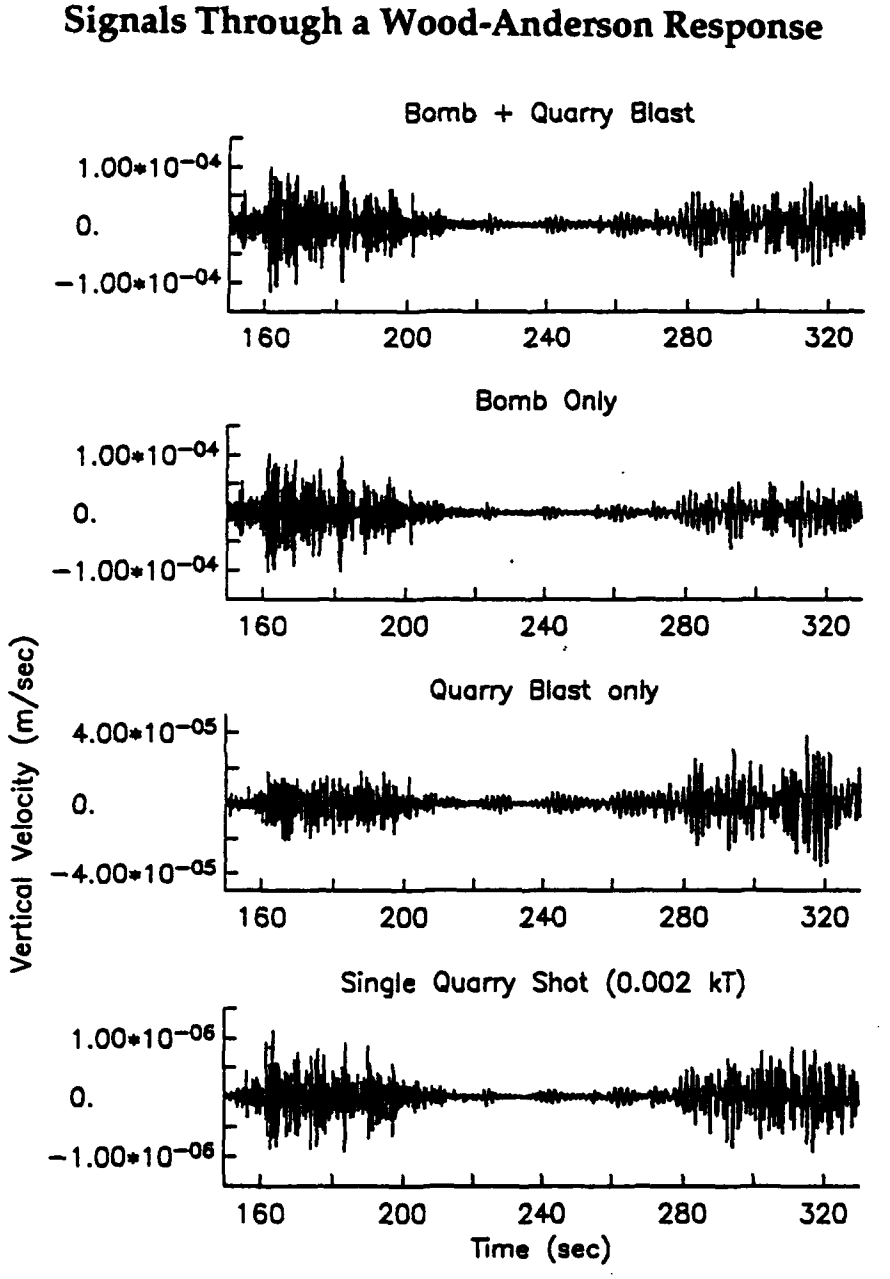

Figure 29. Regional synthetic seismograms filtered with a Wood-Anderson instrument response: from top to bottom; the sum of the quarry blast simulation plus the tamped 1 KT explosion, the tamped 1 KT explosion alone, the quarry blast simulation alone, a single hole in the quarry blast.

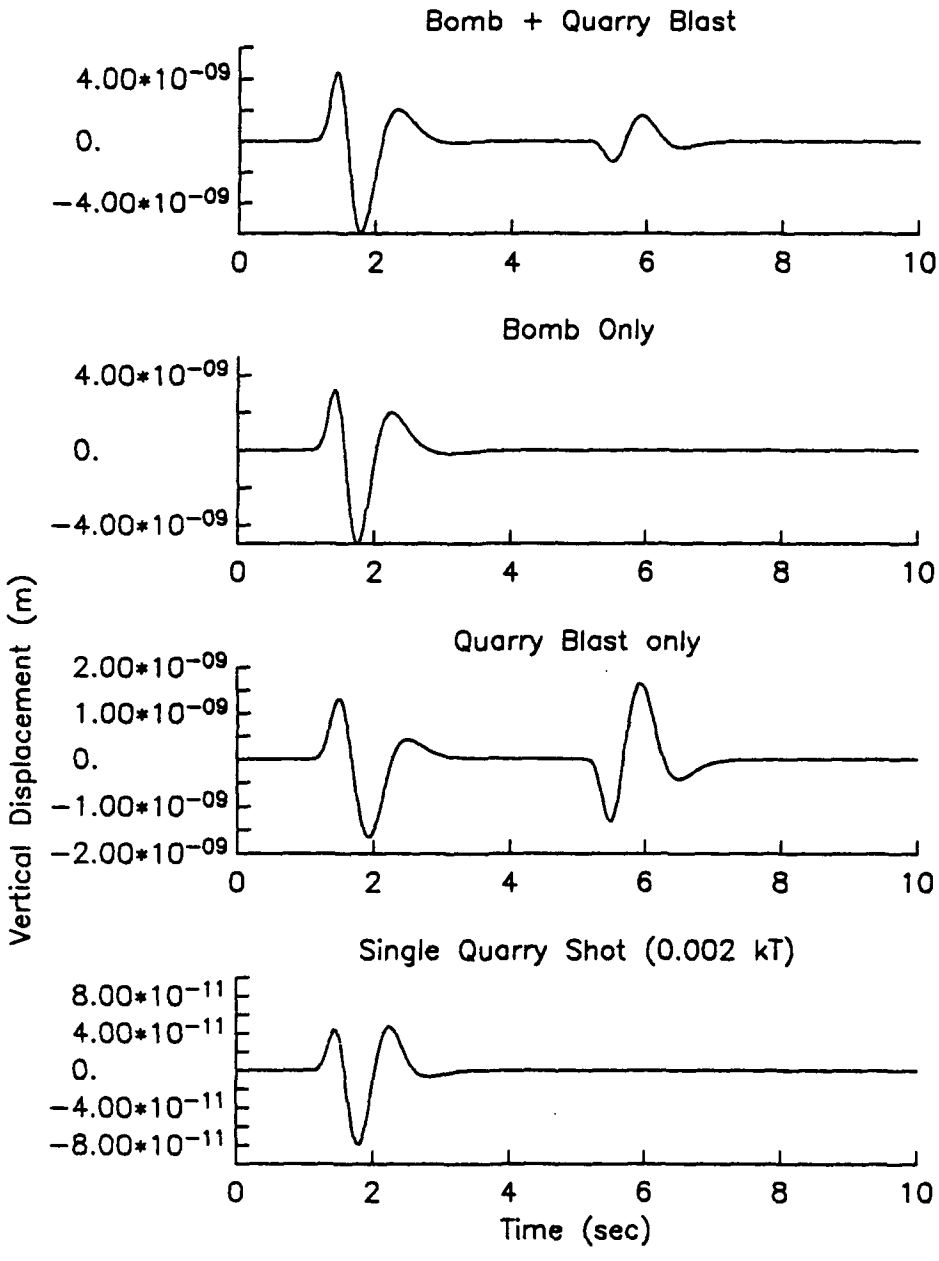

Figure 30. Teleseismic P wave synthetic seismograms filtered with a short period SRO instrument response: from top to bottom; the sum of the quarry blast simulation plus the tamped 1 KT explosion, the tamped 1 KT explosion alone, the quarry blast simulation alone, a single hole in the quarry blast.

charges are larger than those from spall by a factor of about 2 (Figure 31). Using the formulas in Aki and Richards (1980), the m_b for the bomb alone is 4.6, again a reasonable magnitude for a 1 KT explosion. The quarry blast alone has a smaller amplitude and longer period, and an m_b of 4.0.

Note the secondary phase in Figures 30 and 31. This is due to the array response discussed above and shown in Figure 6; there is a signal when the blast starts and a signal of opposite sign when it stops. This is still the case if the array response in Figure 8 (a large scatter in firing times) is used, as shown in Figure 32. The quarry blast could be made to dominate the 1 KT bomb by firing the entire array simultaneously, in which case the amplitude in Figure 30 would be increased by 20. In this case, the secondary phase would not be present.

Signals Through a sp SRO

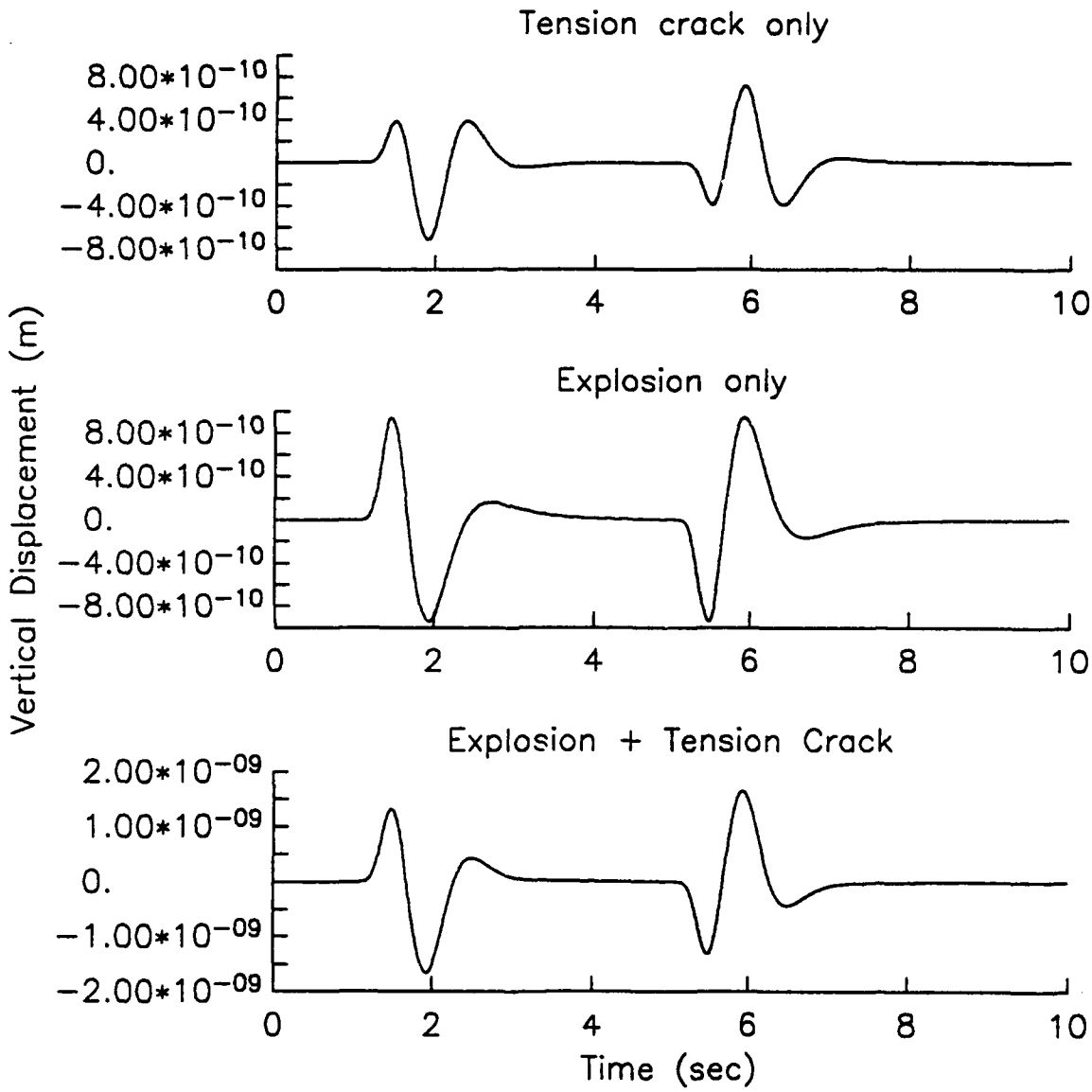

Figure 31. Teleseismic P wave synthetic seismograms of the quarry blast filtered with a short period SRO instrument response showing the contributions of the spall phase alone (top), of the explosive charges (middle) and the sum (bottom).

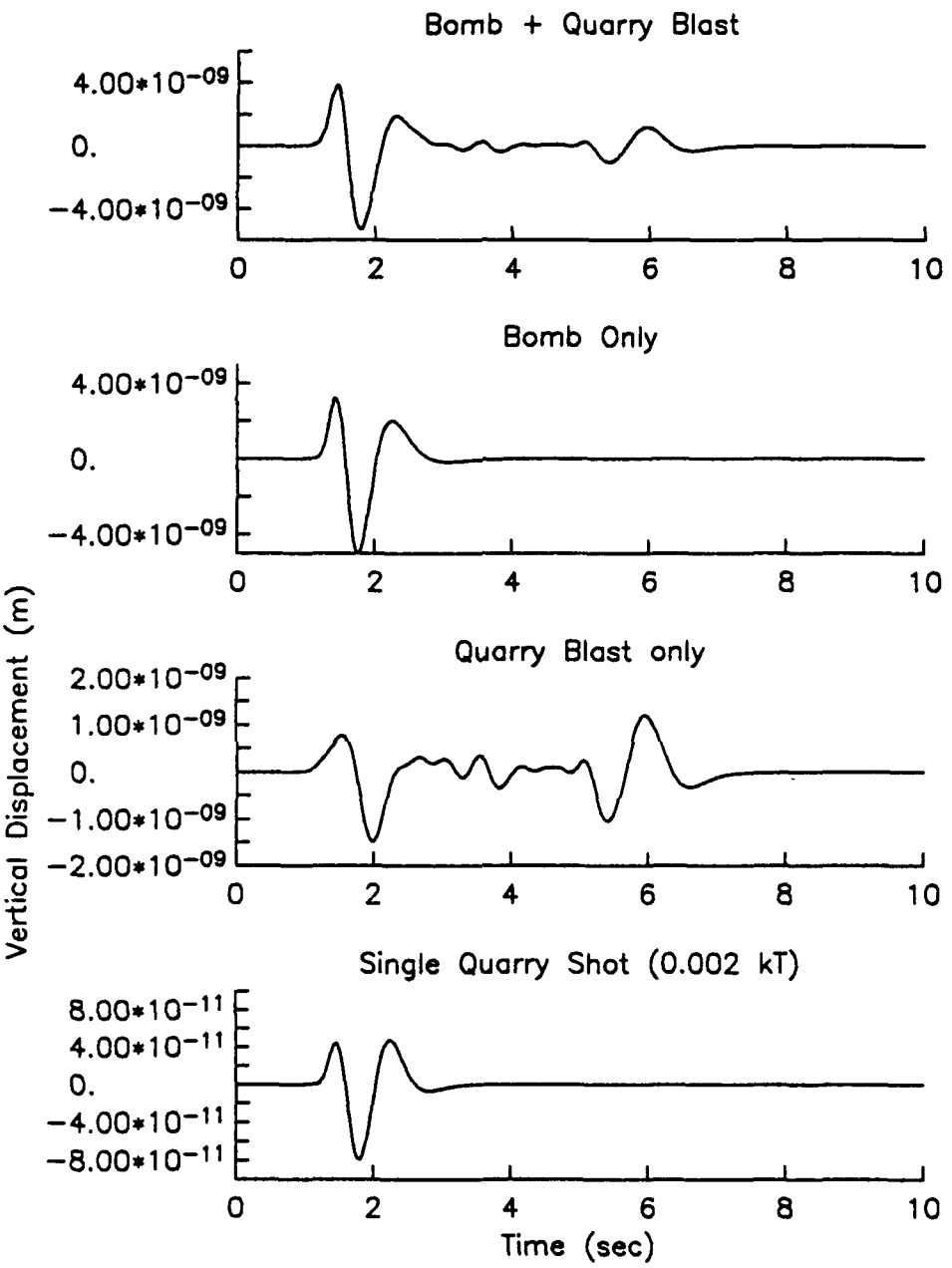

Figure 32. Teleseismic P wave synthetic seismograms filtered with a short period SRO instrument response with a 0.25 sec standard deviation in firing times. From top to bottom; the sum of the quarry blast simulation plus the tamped 1 KT explosion, the tamped 1 KT explosion alone, the quarry blast simulation alone, a single hole in the quarry blast.

3. Conclusions

We have computed synthetic regional and teleseismic seismograms from models of a multiple-shot quarry blast. The charge size, distribution, spall momentum and detonation intervals used in these calculations were chosen to be representative of actual mining practices. We have compared the signals from the quarry blast to signals from overburied nuclear explosions of the same yield. Our calculations show that for regional seismograms of an overburied explosion beneath a one kiloton ripple-fired quarry blast

1. The quarry blast source is band-limited compared to the buried explosion, and decays rapidly over the 0.5-3 Hz frequency band.

2. Pg spectral values rise in the band from 0.5 to 3.5 Hz for the bomb, but fall in that band for the quarry blast,

3. Spall strongly affects the quarry blast source enhancing the generation of Lg and Pg.

4. In a simultaneous explosion and quarry blast, the explosion will dominate the seismic signal if the explosion yield (tamped or equivalent decoupled) exceeds approximately 10 percent of the quarry blast yield.

5. Quarry blast spectral scallops are primarily due to the finite size and duration of the source and are insensitive to the details of the ripple firing timing.

6. Seismic amplitudes from quarry blasts are insensitive to the direction of spall as long as there is minimal elevation change.

7. An elevation change (the spalled quarry face falling to a lower level) can significantly increase seismic amplitudes from quarry blasts. An elevation drop of 10 meters can increase the quarry blast signal by as much as a factor of 5 in the 2-5 Hz frequency band.

We find that for teleseismic signals,

1. the finite duration of the source (or more specifically, the cessation of the source) creates a secondary phase,

2. spall signal amplitudes are about one-third the amplitude of the quarry blast signal, while the explosives account for two-thirds of the amplitude, and

3. the signals from the bomb will dominate if the bomb yield exceeds approximately 30 percent of the quarry blast yield.

4. References

Adushkin, V. V., I. O. Kitov, and D. D. Sultanov (1992), "Experimental Results of USSR Nuclear Decoupling Measurements," Center for Seismic Studies Visiting Scientist Report C92-04, September.

Aki, K. and P.G. Richards (1980), "Quantitative Seismology," W.H. Freeman and Company, San Francisco.

Barker, T.G. and S.M. Day (1990), "A Simple Physical Model for Spall from Nuclear Explosions Based Upon Two-Dimensional Nonlinear Numerical Simulations," S-CUBED Scientific Report to DARPA, SSS-TR-90-11550.

Barker, T.G., K.L. McLaughlin, and J.L. Stevens (1992), "Numerical Models of Quarry Blast Sources," S-CUBED Semiannual Report to DARPA/PL, SSS-TR-92-13515, September.

Chapman, M.C., G.A. Bollinger, and M.S. Sibol (1991), "Spectral Studies of the Elastic Wave Radiation From Appalachian Earthquakes and Explosions Explosion Source Spectra Modeling Using Blaster's Logs," Phillips Laboratory, PL-TR-01-2231.

Day, S.M. and K.L. McLaughlin (1991), "Seismic Source Representations for Spall," *Bull. Seism. Soc. Am., 81, 191-201.*

Day, S.M., N. Rimer and J.T. Cherry (1983), "Surface Waves from Underground Explosions with Spall: Analysis of Elastic and Nonlinear Models," *Bull. Seism. Soc. Am., 73, 247-264.*

Dupont (1942), "Blasters' Handbook," E.I. du Pont de Nemours & Co.

Hedlin, M.A., J.B. Minster and J.A. Orcutt (1990), "An Automatic Means to Discriminate Between Earthquakes and Quarry Blasts," *Bull. Seism. Soc. Am., 80, 6, 2143-2160.*

Langefors, U. and B. Kihlstrom (1963), "The Modern Techniques of Rock Blasting," John Wiley and Sons.

Latter, A. L., R. E. Lelevier, E. A. Martinelli, and W. G. McMillan (1961), "A Method of Concealing Underground Nuclear Explosions," *JGR, 66, 2962.*

McEvilly, T.V. and L.R. Johnson, "Regional Studies with Broadband Data," University of California Report to AFGL, GL-TR-89-0224.

McLaughlin, K. L., T. G. Barker, and S. M. Day (1990), "Implications of Explosion Generated Spall Models: Regional Seismic Signals," S-CUBED Scientific Report No. 2 submitted to Geophysics Laboratory, SSS-TR-90-11535, GL-TR-90-0133, May.

Mueller, R. A. and J. R. Murphy (1971), "Seismic Characteristics of Underground Nuclear Detonations," *Bull. Seism. Soc. Am., 61, 1675-1692.*

Reamer, S.K. and K.-G. Hinzen (1991), "Seismic Study of the Dynamic Response of Rock to Cylindrical Charges Fired in a Half and a Quarter-Space Geometry," in *Proc. of the 17th Conference on Explosives and Blasting Research.*

Reamer, S.K. Hinzen, K.-G. and B.W. Stump (1992), "Near-Source Characterization of the Seismic Wavefield Radiated from Quarry Blasts," *Geophys. J. Int., 110, 435-450.*

Richter, C.F. (1958), "Elementary Seismology," W.H. Freeman and Company, San Francisco.

Smith, A. T. (1992), "Discrimination of Explosions from Simultaneous Mining Blasts," Lawrence Livermore Report UCRL-JC-109245, August.

Stevens, J. L., J. R. Murphy, and N. Rimer (1991), "Seismic Source Characteristics of Cavity Decoupled Explosions in Salt and Tuff," *Bull. Seism. Soc. Am., 81, 4, 1272-1291.*

Stump, B.W. and R.E. Reinke (1988), "Experimental Confirmation of Superposition from Small-Scale Explosions," *Bull. Seism. Soc. Am., 78, 1037-1058.*

Appendix A

A Seismic Source Model for the Quarry Blast Spall Source

K. L. McLaughlin, S. M. Day*, T. G. Barker, and J. L. Stevens
S-CUBED, Division of Maxwell Laboratories, P.O. Box 1620, La Jolla, CA 92038
* San Diego State University, Department of Geological Sciences,
San Diego, CA 92182

The objectives of quarry blasting are to safely shatter and move rock from a quarry face. The rock may then be shifted, loaded, and processed economically. This blasting is accomplished most efficiently by detonating the proper weight of explosives in drill holes at a fixed distance from the face. This distance is referred to as the burden. The charge size and burden are typically chosen so that the burden, Q, divided by the cube-root of the charge weight is between 0.5 and 1 $m/Kg^{1/3}$ (Langefors and Kihlstrom, 1963). It is found that depending upon the type of rock and the geometry of the placement, the blast will spall the mass of rock between the charge hole and the face at between 0.5 and 10 m/s (Langefors and Kihlstrom, 1963). This is not unlike the vertical spall that occurs above contained nuclear explosives, except that most nuclear explosives are detonated at somewhat greater scaled depths of burial, with 120 $m/KT^{1/3}$ = 1.2 $m/Kg^{1/3}$ a typical value. Also, it should be noted that the quarry blast spall is oriented at an arbitrary angle from the horizontal, the free surface may not be flat, and there is a net displacement of the spall mass both horizontally and vertically.

We have found from numerical simulations that the seismic waves excited by spall above nuclear devices can be modeled as either a horizontally oriented tension crack or a set of vertical forces acting on the free surface (Day and McLaughlin, 1991). In this paper we argue that we can model the seismic source from spall in a quarry blast with vertical and horizontal forces on the free surface. The model accommodates the features that the spall is not only vertical, and the spall mass may be horizontally and vertically permanently displaced. The vertical displacement has the added feature that gravitational energy is released in the process. In a later report, we will address the effects that a non-planar free surface may have upon the excitation of seismic waves.

Consider the situation that a volume of rock, V, in a face is moved along a surface Σ (see Figure A-1). We can write the displacement at a far-field location, $\vec{X}$, using the representation theorem (Aki and Richards, 1980),

$$u_i(\vec{X}) = \int_{\Sigma} d\Sigma \, \nu_j(\vec{\eta}) \, \delta u_k(\vec{\eta}) \, C_{jkpq}(\vec{\eta}) \, G_{ip,q}(\vec{X}, \vec{\eta}) \qquad \text{(A-1)}$$

where $u_i(\vec{X})$ is the i'th component of displacement at location $\vec{X}$, $\nu_j(\vec{\eta})$ is the normal at the location $\vec{\eta}$ on the surface Σ, δu_k is the displacement discontinuity across the surface Σ, C_{jkpq} is the elastic tensor, and $G_{ip,q}(\vec{X}, \vec{\eta})$ is the q'th derivative of the Green's tensor response for the i'th component of displacement at $\vec{X}$ given a force in the p'th direction at the location $\vec{\eta}$. Note that from reciprocity we can interpret $T_{ki}(\vec{\eta}, \vec{X}) = \nu_j(\vec{\eta}) \, C_{jkpq}(\vec{\eta}) \, G_{ip,q}(\vec{X}, \vec{\eta})$ as the traction in the k'th direction at $\vec{\eta}$ due to a displacement in the i'th direction at $\vec{X}$.

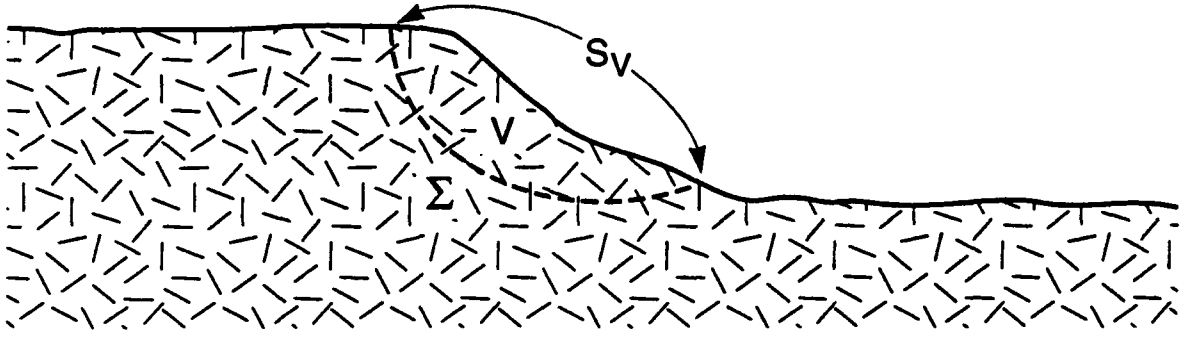

V – Spall Volume

Σ – Spall Surface

S_V – Free Surface of Spall Volume

Figure A-1.

We assume that δu_k is uncorrelated with $C_{jkpq}G_{ip,q}$ on the surface, Σ. We discuss this assumption further below. We can re-write equation (A-l) as

$$u_i(\vec{X}) = \overline{\delta u_k} \int_\Sigma d\Sigma\, \nu_j(\vec{\eta}) C_{jkpq}(\vec{\eta}) G_{ip,q}(\vec{X}, \vec{\eta}) \tag{A-2}$$

where

$$\overline{\delta u_k} = \frac{1}{A_\Sigma} \int_\Sigma d\Sigma\, \nu_j(\vec{\eta}) \delta u_k(\vec{\eta})$$

$$A_\Sigma = \int_\Sigma d\Sigma\ . \tag{A-3}$$

$\overline{\delta u_k}$ is the average displacement discontinuity across the surface, Σ. Since G_{ip} satisfies the equation of motion in V, we can write the equation of motion in the volume V,

$$(C_{jkpq}\, G_{ip,q})_{,j} = -\rho\, \omega^2\, G_{ik}, \tag{A-4}$$

where ρ is the material density and $\omega = 2\pi f$ is the angular frequency. If we now integrate over the volume V,

$$\int_V dv \left(C_{jkpq}\, G_{ip,q}\right)_{,j} = \int_{\Sigma + S_V} d\Sigma\, \nu_j\, C_{jkpq}\, G_{ip,q} = -\omega^2 \int_V dV \rho G_{ik} \tag{A-5}$$

where $\Sigma + S_V$ is the combined surfaces enclosing the volume V. S_V is a free surface, so the integral is zero over S_V and we have that

$$\int_\Sigma d\Sigma\, \nu_j\, C_{jkpq}\, G_{ip,q} = -\omega^2 \int_V dV \rho\, G_{ik}\ . \tag{A-6}$$

Now we denote by $\overline{G_{ik}}$, the average Green's tensor for the mass, m_V,

$$\overline{G_{ik}} = \frac{1}{m_V} \int_V dV\, \rho G_{ik}\ .$$

$$m_V = \int_V dV\, \rho\ , \tag{A-7}$$

and then we can finally conclude that the far-field motion from the material motion at the free surface can be written as

$$u_i(\bar{X}) = -\omega^2 \, \overline{\delta u_k} \, m_V \, \overline{G_{ik}} \; . \qquad \text{(A-8)}$$

Equation (A-8) says that we can represent the quarry spall seismic source by an equivalent set of forces that are proportional to the average acceleration, $-\omega^2 \, \overline{\delta u_k}$, times the mass, m_V, times an average Green's function, $\overline{G_{ik}}$. Note that the acceleration is averaged over the surface of the spall mass while the Green's function is averaged over the volume of the spall mass.

To further interpret hese results, if we define

$$P_k = i\omega \overline{\delta u_k} \, m_V \qquad \text{(A-9)}$$

as the k'th component of the equivalent momentum of the spall mass. Then the equivalent force, F_k, is simply the time derivative of this momentum,

$$u_i(\bar{X}) = -i\omega P_k \overline{G_{ik}} = F_k \overline{G_{ik}} \; . \qquad \text{(A-10)}$$

It is easy to interpret this result. As the material moves away from the face, there is a recoil force. The spall temporarily carries with it the momentum of the material between the shot hole and the free surface. The material then falls, rolls, and/or slides down the face. These resulting impact and frictional forces bring the material to a halt. The recoil and the impact plus frictional forces are in opposite directions. Unlike the nuclear explosion spall, the forces are not vertical since the spall occurs along a face that may be at an arbitrary angle to the vertical. Furthermore, the material above a normally contained nuclear explosion does not experience a significant net offset.

It is interesting to note that since the material may not land in the same place in which it began, the integral of P(t), from t = 0 to t = ∞ may not be zero. This implies that there may be net work done in the rock movement. Furthermore, since the center of gravity of the material may come to rest lower than the initial center of gravity, there may be a net source of gravitational energy for the seismic signal. The velocity gained from a block of rock falling freely 5 meters is comparable to an initial spall velocity of almost 10 m/s. Spall

velocities between 0.5 and 10 m/s are common for quarry blasting. Consequently, it is possible that the gravitational component of the quarry blast spall may be as important as the explosive spall component. Another difference between the spall source of a contained nuclear explosion and that of a quarry blast is that the quarry blast spall often has a well defined horizontal component and hence the radiation pattern from the horizontal forces will not be axisymmetric.

Despite the differences between the quarry blast and contained nuclear explosion spalls, it is interesting to note that equation (A-8) may be used to model the nuclear explosion spall as an equivalent point force on the free surface (see Day and McLaughlin, 1991). Furthermore, since most quarry blasts and contained nuclear explosions are conducted in the same range of scaled depths of burial or scaled depths of burden, the range of velocities of the spalled materials are similar. This leads to similar dwell times for quarry blasts and contained nuclear explosions. The range of 0.5 to 10 m/s in spall velocities corresponds to ballistic times of 0.1 to 2 seconds. Therefore, the characteristic frequencies of spall source time functions are in the same bandwidth for both quarry blasts and contained nuclear explosions.

The model of the quarry blast spall in equation (A-8) adequately describes the effects of the non-horizontal nature of the spall, the action of gravity, and the net displacement of material. The model does not address the problem of the non-planar free-surface. This issue is under study and will be reported later.

We briefly further discuss the conditions that permit the factoring of equation (A-l) to arrive at equation (A-3). The assumption that δu_k is uncorrelated with $C_{jkpq}G_{ip,q}$ on the surface, Σ, is equivalent to the equation

$$\int_{\Sigma} d\Sigma\left(\delta u_k - \overline{\delta u_k}\right)\left(\nu_j C_{jkpq}G_{ip,q} - \overline{\nu_j C_{jkpq}G_{ip,q}}\right) = 0 \qquad \text{(A-11)}$$

where the over bar indicates an average over Σ. Note that from reciprocity we can interpret $T_{ki}\left(\vec{\eta},\vec{X}\right) = \nu_j(\vec{\eta})C_{jkpq}(\vec{\eta})G_{ip,q}\left(\vec{X},\vec{\eta}\right)$ as the traction in the k'th direction at $\vec{\eta}$ due to a displacement in the i'th direction at $\vec{X}$.

We can interpret the above equation as saying that the displacement discontinuity on the surface, δu_k, is well represented by its average, $\overline{\delta u_k}$. This

seems a reasonable assumption, since the excitation by the variations in the displacement discontinuity from the average will only excite high frequency waves that tend to cancel out. Or alternatively, we can interpret this equation as saying that the tractions on the surface from a far-field source, T_{ki}, are well represented by their average value over the surface, $\overline{T_{ki}}$. This later interpretation is certainly the case for wavelengths much longer than the size of the spall surface.

If these conditions are met then we can write,

$$\int_{\Sigma} d\Sigma\, \delta u_k\, \nu_j\, C_{jkpq}\, G_{ip,q} = \overline{\delta u_k} \int_{\Sigma} d\Sigma\, \nu_j\, C_{jkpq}\, G_{ip,q}, \qquad \text{(A-12)}$$

which leads to equation (A-2).

References

Aki, K., and P. G. Richards (1980). Quantitative Seismology, Vol. I, W. H. Freeman and Co., San Francisco.

Day, S. M., and K. L. McLaughlin (1991). Seismic Source Representations for Spall, Bull. Seism. Soc. Am., 81, 191-201.

Langefors, U. and B. Kihlstrom (1963). The Modern Technique of Rock Blasting, John Wiley and Sons, New York, 405pp.